

1 RESEARCH ARTICLE

2 **The transcription factors ZmNAC128 and ZmNAC130 coordinate**  
3 **with Opaque2 to promote endosperm filling in maize**

4  
5 Erwang Chen<sup>1#</sup>, Huiqin Yu<sup>1#</sup>, Juan He<sup>1#</sup>, Di Peng<sup>1#</sup>, Panpan Zhu<sup>1</sup>, Shuxing Pan<sup>1</sup>,  
6 Xu Wu<sup>1</sup>, Jincang Wang<sup>1</sup>, Chen Ji<sup>2</sup>, Zhenfei Chao<sup>2</sup>, Zhuopin Xu<sup>3</sup>, Yuejin Wu<sup>3</sup>,  
7 Daiyin Chao<sup>2</sup>, Yongrui Wu<sup>2</sup> and Zhiyong Zhang<sup>1\*†</sup>

8  
9 <sup>1</sup>School of Life Sciences, Division of Life Sciences and Medicine, University of  
10 Science and Technology of China, Hefei 230027, China

11 <sup>2</sup>National Key Laboratory of Plant Molecular Genetics, CAS Center for Excellence in  
12 Molecular Plant Sciences, Shanghai Institute of Plant Physiology and Ecology,  
13 Chinese Academy of Sciences, Shanghai 200032, China

14 <sup>3</sup>Anhui Key Laboratory of Environmental Toxicology and Pollution Control  
15 Technology, Hefei Institutes of Physical Science, Chinese Academy of Sciences,  
16 Hefei, Anhui 230031, China

17  
18 <sup>#</sup>These authors contributed equally to this work

19 <sup>\*</sup>Corresponding author: zhiyong2@ustc.edu.cn

20 <sup>†</sup>Senior author

21  
22 **Short Title:** Three core TFs control endosperm filling

23  
24  
25  
26  
27  
28 The author responsible for distribution of materials integral to the findings presented  
29 in this article in accordance with the policy described in the Instructions for Authors  
30 (<https://academic.oup.com/plcell/pages/General-Instructions>) is: Zhiyong Zhang  
31 (zhiyong2@ustc.edu.cn).

32

33 **Keywords:** Maize, Grain filling, ZmNAC128, ZmNAC130, Opaque2

34

35 **Abstract**

36 Endosperm filling in maize (*Zea mays*), which involves nutrient uptake and  
37 biosynthesis of storage reserves, largely determines grain yield and quality. However,  
38 much remains unclear about the synchronization of these processes. Here, we  
39 comprehensively investigated the functions of duplicate NAC-type transcription  
40 factors, namely ZmNAC128 and ZmNAC130, in endosperm filling. The gene-edited  
41 double mutant *zmnac128 zmnac130* exhibits a poorly filled kernel phenotype such  
42 that the kernels have an inner cavity. RNA sequencing and protein abundance analysis  
43 revealed that the expression of many genes involved in the biosynthesis of zein and  
44 starch is reduced in the filling endosperm of *zmnac128 zmnac130*. Further DNA  
45 affinity purification and sequencing combined with chromatin-immunoprecipitation  
46 quantitative PCR and promoter transactivation assays demonstrated that ZmNAC128  
47 and ZmNAC130 are direct regulators of three (16-, 27-, and 50-kD)  $\gamma$ -zein genes and  
48 six important starch metabolism genes (*Brittle2* [*Bt2*], *pullulanase-type starch*  
49 *debranching enzyme* [*Zpu1*], *granule-bound starch synthase 1* [*GBSSI*], *starch*  
50 *synthase 1* [*SSI*], *starch synthase IIa* [*SSIIa*], and *sucrose synthase 1* [*Sus1*]).  
51 ZmNAC128 and ZmNAC130 recognize an additional cis-element in the *Opaque2* (*O2*)  
52 promoter to regulate its expression. The triple mutant *zmnac128 zmnac130 o2* exhibits  
53 extremely poor endosperm filling, which results in more than 70% of kernel weight  
54 loss. ZmNAC128 and ZmNAC130 regulate the expression of the transporter genes  
55 *sugars will eventually be exported transporter 4c* (*ZmSWEET4C*), *sucrose and*  
56 *glucose carrier 1* (*ZmSUGCAR1*), and *yellow stripe-like2* (*ZmYSL2*) and in turn  
57 facilitate nutrient uptake, while *O2* plays a supporting role. In conclusion,  
58 ZmNAC128 and ZmNAC130 cooperate with *O2* to facilitate endosperm filling, which  
59 involves nutrient uptake in the basal endosperm transfer layer (BETL) and the  
60 synthesis of zeins and starch in starchy endosperm (SE).

61

62

63 **IN A NUTSHELL**

64 **Background:** Cereal endosperms store starch and proteins in grains and play a critical  
65 role in determining grain yield and quality. Maize (*Zea mays*), with its sizable grain, is  
66 an excellent model for studying cereal endosperm development. Endosperm filling  
67 involves two synchronized processes: maternal-to-endosperm nutrient transfer and  
68 storage reserve biosynthesis. Several important nutrient transfer-related genes have  
69 been identified, and the regulation of storage reserve biosynthesis has been broadly  
70 studied in maize. Notably, the transcription factor-encoding genes *Opaque2* (*O2*),  
71 *ZmNAC128*, and *ZmNAC130* exhibit strong expression in the filling endosperm.  
72 However, how these three transcription factors co-regulate the synchronization of  
73 these endosperm-filling processes remains elusive.

74

75 **Question:** What are the roles of *ZmNAC128* and *ZmNAC130* in endosperm filling?  
76 How do they function together with *O2* in this process?

77

78 **Findings:** *ZmNAC128* and *ZmNAC130* directly regulate the expression of all  $\gamma$ -*zein*  
79 genes (encoding storage proteins) and multiple important starch metabolism genes,  
80 making them pivotal coordinators of grain quality and yield. Furthermore,  
81 *ZmNAC128* and *ZmNAC130* directly regulate the expression of *O2*, and together  
82 these three transcription factors synergistically activate their own expression through  
83 autoregulation and physical interactions. *ZmNAC128* and *ZmNAC130* also regulate  
84 the expression of vital transporter genes responsible for facilitating nutrient transfer  
85 from the mother plant to the endosperm. This regulatory mechanism enhances nutrient  
86 uptake, with *O2* playing a supportive role.

87

88 **Next steps:** We plan to identify additional co-regulatory factors involved in  
89 endosperm filling to gain a comprehensive understanding of endosperm filling, from  
90 nutrient uptake to the biosynthesis of storage reserves.

91

92 **Introduction**

93 Cereal grain endosperms, which serve as the main storage site of starch and  
94 proteins in kernels, account for approximately 90% of kernel weight (Flint-Garcia et  
95 al., 2009). The endosperm supports embryogenesis and seed germination during early  
96 seedling development, while the endosperm is also a main source of food, feed, and

97 industrial raw materials worldwide (Flint-Garcia, 2017; Hannah and Boehlein, 2017;  
98 Huang et al., 2021). Among cereals, maize (*Zea mays*) has the largest caryopsis,  
99 making it an excellent model species for investigating endosperm development  
100 (Sabelli and Larkins, 2009). Like that of other cereal grains, maize endosperms start  
101 to develop after double fertilization, wherein one sperm fertilizes the diploid central  
102 cell to initiate the formation of the triploid endosperm (Sabelli and Larkins, 2009).

103 Endosperm development involves three typical physiological stages: early,  
104 middle, and mature stages. During the early stage, the fertilized endosperm undergoes  
105 coenocyte formation, cellularization, and differentiation (Olsen, 2001). Seven  
106 distinguishable compartments are formed by approximately 8 d after pollination  
107 (DAP): starchy endosperm (SE), aleurone (AL), embryo surrounding region (ESR),  
108 basal endosperm transfer layer (BETL), basal-intermediate zone (BIZ), conducting  
109 zone (CZ), and sub-aleurone (SA) (Olsen, 2001; Becraft and Gutierrez-Marcos, 2012;  
110 Leroux et al., 2014; Zhan et al., 2017; Dai et al., 2021). Endosperm cell fate is largely  
111 determined during this stage. Starting at approximately 8-10 DAP, endosperm  
112 development is accompanied by the coordination of maternal-to-filial nutrient transfer  
113 in the BETL and the synthesis of storage reserves in the SE, which ultimately  
114 determine the yield and quality of the kernel. Subsequently, kernels gradually  
115 dehydrate and mature.

116 In recent years, spatiotemporal high-resolution transcriptome analyses and  
117 advanced functional genomic studies have greatly advanced our understanding of  
118 endosperm development in maize (Xin et al., 2013; Chen et al., 2014; Zhan et al.,  
119 2015; Yi et al., 2019; Li and Wu, 2020). For instance, the BETL at the base of the  
120 endosperm is the gateway through which nutrients are transported to the central SE, a  
121 process that is facilitated by the BIZ and CZ compartments (Chourey and Hueros,  
122 2017). When mutated, BETL-specific sugar transfer-related genes including  
123 *Miniature1* (*ZmMN1*, encoding CELL WALL INVERTASE2) (Cheng et al., 1996),  
124 *Sugars will eventually be exported transporter 4c* (*ZmSWEET4c*) (Sosso et al., 2015),  
125 and *Sucrose and glucose carrier 1* (*ZmSUGCAR1*, also referred to as *ZmNPF7.9*

126 [*Nrt1/Ptr family 7.9*] and *ZmMN2*) largely block mother-to-endosperm sugar transfer  
127 and the synthesis of storage reserves (Guan et al., 2020; Wei et al., 2021; Zhou et al.,  
128 2021; Yang et al., 2022a). Recently, the *shrunken4 (sh4)* mutant was shown to harbor  
129 a mutation in the oligopeptide metal transporter YELLOW STRIPE-LIKE2  
130 (*ZmYSL2*), which predominantly exists in the AL and BETL compartments (He et al.,  
131 2021; Chao et al., 2022). Like mutants with defects in sugar transporter genes  
132 expressed in the BETL, the *sh4* mutant also exhibits a shrunken-kernel phenotype,  
133 suggesting that *ZmYSL2* is critical for endosperm filling. MYB-RELATED  
134 PROTEIN1 (MRP1) is an important transcription factor (TF) for BETL development  
135 and function (Gomez et al., 2002; Gomez et al., 2009); loss-of-function mutants are  
136 needed to determine its role during grain filling.

137 The SE compartment occupies the largest part of the endosperm and is the site of  
138 the biosynthesis and deposition of storage reserves during the filling stage.  
139 Ultramicroscopy observations of filling-stage and mature endosperms revealed that  
140 the SE is filled with two types of storage bodies: starch granules (SGs) and protein  
141 bodies (PBs) (Sabelli and Larkins, 2009). SGs are formed by the orderly assembly of  
142 starch in amyloplasts (Hannah and Boehlein, 2017). Starch accounts for  
143 approximately 70% of dry kernel weight, so its content is closely related to yield. PBs,  
144 which are insoluble and spherical, are formed by the synthesis and deposition of zeins  
145 (the most abundant seed storage proteins in maize) within the lumen of the rough  
146 endoplasmic reticulum (Lending and Larkins, 1989; Larkins et al., 2017). Zeins lack  
147 several essential amino acids (lysine, tryptophan, and methionine), which greatly  
148 affects seed protein quality (Larkins et al., 2017). Temporal high-resolution  
149 transcriptome analyses of endosperm development have indicated that genes encoding  
150 zeins and enzymes participating in starch biosynthesis are specifically and strongly  
151 expressed during the filling stage (Chen et al., 2014). This suggested that common  
152 TFs or regulators might contribute to their synchronized biosynthesis.

153 The first TF identified related to zein biosynthesis was Opaque2 (O2), which  
154 directly regulates the expression of *22-kD  $\alpha$ -zein* through the recognition of the

155 O<sub>2</sub>-box cis-element in its promoter (Schmidt et al., 1987; Schmidt et al., 1990).  
156 Analysis of differentially expressed genes (DEGs) in the *o2* mutant, combined with  
157 genome-wide chromatin immunoprecipitation followed by deep sequencing  
158 (ChIP-seq), revealed that O<sub>2</sub> regulates the expression of most zein genes, with the  
159 exception of the *16-kD*  $\gamma$ -zein gene (Li et al., 2015; Zhan et al., 2018). ZmNAC128  
160 and ZmNAC130 were recently shown to regulate the expression of *16-kD*  $\gamma$ -zein via  
161 their ability to bind to a specific cis-element (ACGCAA) in its promoter (Zhang et al.,  
162 2019), although it remains unknown whether or how these two NACs regulate the  
163 expression of other zein genes. The 27-kD  $\gamma$ -zein is involved in the initiation of PB  
164 formation (Wu et al., 2010), and its expression is regulated by a complex series of TFs,  
165 including BASIC LEUCINE ZIPPER22 (ZmbZIP22) (Li et al., 2018),  
166 PROLAMIN-BOX BINDING FACTOR1 (PBF1) (VicenteCarbajosa et al., 1997; Wu  
167 and Messing, 2012), O<sub>2</sub> HETERODIMERIZING PROTEINS (OHP1 and OHP2)  
168 (Pysh et al., 1993; Zhang et al., 2015), and O<sub>2</sub> (Li et al., 2015). Upon the interaction  
169 with O<sub>2</sub>, ZmMADS47, a MADS box-containing TF, binds to the CATGT motif in the  
170 promoters of  $\alpha$ -zein and *50-kD*  $\gamma$ -zein for their transactivation (Qiao et al., 2016). In  
171 general, O<sub>2</sub> appears to be a core TF that regulates the expression of zein genes  
172 through additive and synergistic interactions with multiple TFs, including ZmbZIP22,  
173 PBF1, OHP1, OHP2, and ZmMADS47.

174 Among the characterized TFs regulating the expression of zein genes, some also  
175 directly regulate the expression of genes encoding enzymes in the starch biosynthesis  
176 pathway. Our previous studies demonstrated that O<sub>2</sub> coordinates the expression of  
177 important starch metabolism genes, including *starch synthase III (SSIII)*, the three  
178 major sucrose synthases (*sucrose synthase Sh1 [Shrunken1]*, *sucrose synthase 1*  
179 [*Sus1*], and *Sus2*), and *pyruvate orthophosphate dikinase (PPDK)* (Zhang et al., 2016;  
180 Deng et al., 2020). Knockdown of *ZmNAC128* and *ZmNAC130* via RNA interference  
181 (RNAi) significantly downregulated the expression of multiple starch metabolism  
182 genes. Among these genes, *Brittle2 (Bt2)*, which encodes the adenosine diphosphate  
183 glucose pyrophosphorylase (AGPase) small subunit, is a direct downstream target of

184 ZmNAC128 and ZmNAC130 (Zhang et al., 2019).

185       Although ZmNAC128 and ZmNAC130 are also important coordinators of the  
186 synchronized synthesis of zeins and starch, their gene regulatory networks (GRN)  
187 remain largely unknown. Additionally, Opaque11 (O11), a hub TF for endosperm  
188 development, also directly regulates the expression of carbohydrate-related genes  
189 (*starch synthase V* [*SSV*] and *pyruvate kinase*) (Feng et al., 2018). Moreover, NAKED  
190 ENDOSPERM1 (NKD1) and NKD2 directly or indirectly regulate the expression of  
191 zein genes, and are also predicted to act as transcriptional activators of *starch synthase*  
192 *1* (*SSI*), *sugary1* (*Su1*), and *waxy* (*Wx*) (Gontarek et al., 2016). We do not yet clearly  
193 understand the transcriptional regulation of starch metabolism genes in the endosperm.  
194 One way to fill this gap is to identify additional TFs that regulate starch metabolism  
195 via forward or reverse genetics; another complementary approach is to determine the  
196 GRN of the identified TFs, such as ZmNAC128 and ZmNAC130 or NKD1 and  
197 NKD2, by DEG analysis in their respective mutants combined with global cis-element  
198 characterization. Such an approach successfully revealed the GRN of O2 and PBF1  
199 through the combined analysis of DEGs and genome-wide ChIP-seq by different  
200 groups (Li et al., 2015; Zhan et al., 2018; Ning et al., 2022).

201       In general, endosperm filling has been intensively investigated over the past few  
202 decades, and progress has been made in understanding the regulation of storage  
203 proteins and starch, nutrient transfer, and initiation of filling. However, the  
204 synchronization of these events during grain filling remains poorly understood. O2,  
205 *ZmNAC128*, and *ZmNAC130* are the most highly expressed TF-encoding genes in the  
206 filling-stage endosperm (Chen et al., 2014). O2 has been comprehensively  
207 investigated in recent decades, but ZmNAC128 and ZmNAC130 remain poorly  
208 understood. This study aims to shed light on the roles of ZmNAC128, ZmNAC130,  
209 and O2 in regulating endosperm filling. These roles encompass the coordination of  
210 zeins and starch synthesis, maintaining their own high expression levels, and  
211 regulating the expression of critical transporter genes in the BETL

212

## 213 **Results**

### 214 **ZmNAC128 and ZmNAC130 are essential for endosperm filling**

215 Our previous study found that knockdown of expression of *ZmNAC128* and  
216 *ZmNAC130* via RNA interference (RNAi) caused a shrunken kernel phenotype with  
217 30% of kernel weight loss, while a *zmnac130* mutant of a five-amino acids deletion  
218 within the conserved NAC domain of its encoding protein did not lead to any apparent  
219 kernel phenotype. Meanwhile, ZmNAC128 and ZmNAC130 could recognize the  
220 same cis-element ACGCAA to co-regulate the expression of *16-kD  $\gamma$ -zein* and *Bt2*,  
221 which suggests their functional redundancy (Zhang et al., 2019). However, the  
222 contribution by ZmNAC128 and ZmNAC130 to endosperm filling remains largely  
223 unknown.

224 Therefore, knockout mutants of *ZmNAC128* and *ZmNAC130* were generated by  
225 clustered regularly interspaced short palindromic repeats  
226 (CRISPR)/CRISPR-associated nuclease 9 (Cas9)-mediated gene editing in this study.  
227 We obtained three independent knockout mutants, each of which had a different  
228 frameshift mutation: *zmnac128-1*, *zmnac128-2*, *zmnac128-3*, *zmnac130-1*,  
229 *zmnac130-2*, and *zmnac130-3* (Supplemental Figure S1). The six single mutants  
230 exhibited normal cob and kernel phenotypes similar to the wild type (WT) KN5585.  
231 However, all double mutants of different allele combinations of *zmnac128* and  
232 *zmnac130* exhibited the same poorly filled-kernel phenotype (Supplemental Figure  
233 S1). Among these knockout mutants, *zmnac128-1*, *zmnac130-1*, and *zmnac128-1*  
234 *zmnac130-1*, which were abbreviated as *zmnac128*, *zmnac130*, and *zmnac128*  
235 *zmnac130* hereafter, were used for subsequent studies.

236 Observations of kernel longitudinal sections revealed a cavity within the  
237 endosperm of *zmnac128 zmnac130* and its peripheral endosperm became floury, while  
238 kernel phenotypes of the single mutants *zmnac128* and *zmnac130* were the same as  
239 that of the WT (Figure 1A). Scanning electron microscopy (SEM) observations  
240 indicated that the SGs are smaller in the endosperm of *zmnac128 zmnac130* than in  
241 that of the WT (Figure 1A). The hundred-kernel weight (HKW) of *zmnac128*



242 *zmnac130* was 56.8% lower than that of the WT, while the HKW of *zmnac128* and  
243 *zmnac130* was not significantly reduced (Figure 1B). Although their RNAi mutants  
244 (*nacRNAi*) also caused 30% of kernel weight loss compared to the corresponding  
245 nontransgenic (NT) kernels (Zhang et al., 2019), it is obvious that knockout of  
246 *ZmNAC128* and *ZmNAC130* lead to even lower kernel weight and more severe kernel  
247 phenotypes than that of *nacRNAi*.

248 Furthermore, we analyzed the protein and starch contents in mature kernels via  
249 near-infrared (NIR) spectroscopy analysis (Figure 1C). The starch contents in the  
250 kernels of the two single mutants were slightly but significantly reduced, while the  
251 protein content in the kernels of *zmnac128* was also slightly reduced with a significant  
252 difference. However, the contents of protein and starch in the kernels of *zmnac128*  
253 *zmnac130* decreased by more than 50% compared to those of the WT and were also  
254 lower than those of *nacRNAi* (Zhang et al., 2019). Therefore, these knockout mutants  
255 generated in this study are a prerequisite for comprehensively investigating the  
256 function of *ZmNAC128* and *ZmNAC130* in the endosperm filling. These results  
257 clearly pointed out that *ZmNAC128* and *ZmNAC130* redundantly promote  
258 endosperm filling, as their simultaneous loss of function severely impaired the  
259 accumulation of storage reserves.

## 260 **RNA-seq combined with DAP-seq facilitates the functional dissection of** 261 ***ZmNAC128* and *ZmNAC130***

### 262 **DEG analysis of *zmnac128 zmnac130* indicates the enrichment of zein and** 263 **starch metabolism**

264 To study the GRN of *ZmNAC128* and *ZmNAC130*, we conducted RNA  
265 sequencing (RNA-seq) analysis using total RNA extracted from 16-DAP endosperms  
266 of WT, *zmnac128*, *zmnac130*, and *zmnac128 zmnac130* in the KN5585 background.  
267 We identified DEGs in the three mutants relative to the WT based on the selection  
268 criteria of a fold-change (FC)  $\geq 2$  and a *p*-value  $\leq 0.05$ . Only 80 and 2 DEGs were  
269 detected in *zmnac128* and *zmnac130*, respectively. However, this number rose to  
270 2,686, with 1,529 upregulated and 1,157 downregulated genes in *zmnac128 zmnac130*

271 (Figure 2A and Supplemental Dataset S1). This result further supported the functional  
272 redundancy of the two NACs.

273 We performed an enrichment analysis of Gene Ontology (GO) terms and Kyoto  
274 Encyclopedia of Genes and Genomes (KEGG) pathways based on the DEGs in  
275 *zmnac128 zmnac130*. We observed two significantly enriched GO terms for molecular  
276 function, one of which was “nutrient reservoir activity” (GO:0045735,  $p$ -value =  
277 2.17E-06), which mainly included zein family genes (Figure 2B). Indeed, the  
278 expression of all zein family genes was significantly downregulated to varying extents  
279 in *zmnac128 zmnac130* (Supplemental Table S1). Moreover, multiple carbohydrate  
280 metabolism-related pathways were enriched (Figure 2B). These results suggested that  
281 ZmNAC128 and ZmNAC130 play crucial roles in the biosynthesis of zeins and  
282 starch.

### 283 **DAP-seq reveals genome-wide binding features of ZmNAC128 and** 284 **ZmNAC130**

285 DNA affinity purification and sequencing (DAP-seq) is a recently developed  
286 method of genome-wide TF-binding site identification, which is fast, inexpensive, and  
287 more easily scaled than ChIP-seq and bypasses the difference of sampling stage  
288 (Bartlett et al., 2017 and Galli et al., 2018). In this study, we conducted the DAP-seq  
289 assay by incubation of recombinant purified ZmNAC128 and ZmNAC130 proteins  
290 and the use of a DNA library prepared from genomic DNA extracted from 16-DAP  
291 endosperms of the reference inbred line B73. The Model-based Analysis of ChIP-Seq  
292 (MACS) (Zhang et al., 2008) under the threshold of  $q$ -value  $\leq 0.05$  revealed 14,211  
293 peaks for ZmNAC128 and 9,261 peaks for ZmNAC130 (Supplemental Dataset S2), of  
294 which 7,082 peaks were common between the two NACs. We determined that  
295 approximately 60% of all the peaks bound by the two NACs were in the genic region  
296 approximately 3 kb from the transcription start site (TSS), of which more than 40%  
297 (4,811 genes) were within 1 kb of the TSS (Figure 2C). Further analysis showed that  
298 the peaks were strongly concentrated immediately upstream of the TSS (Figure 2D),  
299 consistent with the function of ZmNAC128 and ZmNAC130 as TFs.

300 To identify putative target genes of ZmNAC128 and ZmNAC130, these 4,811  
301 genes with NAC-binding peaks around 1 kb of TSS were overlapped with DEGs of  
302 *zmnac128 zmnac130* versus the WT in the KN5585 genetic background. Venn  
303 diagram results showed that 248 upregulated and 250 downregulated genes  
304 overlapped as putative direct targets (Supplemental Figure S2 and Supplemental  
305 Dataset S3). These identified genes were further compared with DEGs of *zmnac128*  
306 *zmnac130* in the KN5585 × B73 background of this study, of which 138  
307 downregulated and 64 upregulated genes were common to both genetic backgrounds  
308 (Supplemental Dataset S4). They included multiple plant hormone-related genes, TFs,  
309 putative transporters, sugar metabolism genes, and so on. Among them, the two amino  
310 acid metabolism genes, *proline oxidase* (Zm00001eb022980) and *lysine-ketoglutarate*  
311 *reductase/saccharopine dehydrogenase 1 (LKR/SDH1)*, Zm00001eb192910), are not  
312 only the potential targets of ZmNAC128 and ZmNAC130 but also the direct targets of  
313 O2 (Li et al., 2015 and Zhan et al., 2018).

#### 314 **ZmNAC128 and ZmNAC130 bind to the promoters of 16-kD $\gamma$ -zein and Bt2**

315 *16-kD  $\gamma$ -zein* and *Bt2* were previously identified as direct target genes of the two  
316 NACs (Zhang et al., 2019). Visualization of the DAP-seq data by the Integrated  
317 Genomics Viewer (IGV) showed that the identified cis-element ACGCAA was  
318 surrounded by binding peaks for ZmNAC128 and ZmNAC130 in the promoters of  
319 *16-kD  $\gamma$ -zein* and *Bt2* (Figure 2E). This suggested that our DAP-seq data are robust for  
320 the detection of potential target genes. We thus explored the genome-wide  
321 cis-elements bound by the two NACs via the motif discovery tool MEME-ChIP. The  
322 most significant cis-element bound by ZmNAC128 and ZmNAC130 was ACGCAA  
323 (E-value < 5.7E-149) (Figure 2F), which was identical to the previously identified  
324 cis-element in the promoters of *16-kD  $\gamma$ -zein* and *Bt2* (Zhang et al., 2019). In addition  
325 to this motif, multiple candidate binding motifs were detected by DAP-seq  
326 (Supplemental Figure S3). These candidates were highly identical either in the two  
327 independent replicates or between ZmNAC128 and ZmNAC130, suggesting that the  
328 two NACs also recognize other cis-elements in addition to the ACGCAA motif.

329 Although multiple enriched elements are commonly detected in the DAP-seq analysis  
330 of ZmNAC128 and ZmNAC130, some of them could be binding motifs for their  
331 cofactors. For instance, the core motif ‘ACGT’ recognized by bZIP-type TFs (such as  
332 O2) is also enriched in the DAP-seq of ZmNAC128 and ZmNAC130, but it requires  
333 additional investigation.

### 334 ***27-kD* and *50-kD* $\gamma$ -zein are direct targets of ZmNAC128 and ZmNAC130**

335 Consistent with the downregulated expression of all zein family genes in  
336 *zmnac128 zmnac130* (Supplemental Table S1), overall zein protein abundance was  
337 also lower in mature kernels of *zmnac128 zmnac130*, with the 16-kD  $\gamma$ -zein protein  
338 being nearly undetectable (Supplemental Figure S4). These results thus supported the  
339 notion that, in addition to O2, ZmNAC128 and ZmNAC130 are also core TFs  
340 involved in zein gene expression. To investigate the regulation of ZmNAC128 and  
341 ZmNAC130 on the expression of other zein genes, we examined the DAP-seq data in  
342 detail. We observed peaks corresponding to the binding of ZmNAC128 and  
343 ZmNAC130 in the promoters of the other two  $\gamma$ -zein genes, *27-kD* and *50-kD*  $\gamma$ -zein  
344 (Figure 3A). We detected the conserved motif ACGCAA around the binding peak  
345 regions in the promoters at -1,421/-1,464 and -461 bp upstream from the start codon  
346 of *27-* and *50-kD*  $\gamma$ -zein genes, respectively (Figure 3A).

347 To test the binding of ZmNAC128 and ZmNAC130 to the fragments containing  
348 ACGCAA in the two promoters, we performed the ChIP-qPCR assay. For this assay,  
349 we used an antibody against the Flag tag and the 16-DAP endosperms of the  
350 transgenic lines of 3×Flag-tagged ZmNAC128 and ZmNAC130 that are driven by the  
351 *27-kD*  $\gamma$ -zein promoter (Supplemental Figure S5). The ChIP-qPCR results verified the  
352 binding relationship of ZmNAC128 and ZmNAC130 in the two  $\gamma$ -zein gene  
353 promoters revealed by our DAP-seq analysis (Figure 3B). A dual-luciferase reporter  
354 (DLR) assay was thus performed to assess the transactivation activities of  
355 ZmNAC128 and ZmNAC130 for the expression of firefly luciferase (LUC)-encoding  
356 gene driven by the two promoters in maize leaf protoplast cells. Compared to the  
357 empty vector control, LUC activities driven by the *27-kD*  $\gamma$ -zein promoter could be

358 significantly increased by the co-transformation of 35S promoter-driven *ZmNAC128*  
359 or *ZmNAC130*. Similarly, LUC activities driven by the *50-kD*  $\gamma$ -zein promoter were  
360 also significantly increased by *ZmNAC128* or *ZmNAC130* (Figure 3C). Similar to the  
361 *16-kDa*  $\gamma$ -zein promoter (Zhang et al., 2019), LUC activities driven by the two  
362 promoters were not stronger under the co-expression of both *ZmNAC128* and  
363 *ZmNAC130* (Figure 3C).

364 Combining these results with our previous findings (Zhang et al., 2019), we  
365 concluded that *ZmNAC128* and *ZmNAC130* are direct transcriptional regulators of  
366 all three (*50-*, *27-*, and *16-kD*)  $\gamma$ -zein genes. We previously found that the PB number  
367 is significantly reduced in the filling endosperm of *nacRNAi* lines (Zhang et al., 2019).  
368 As  $\gamma$ -zein proteins are essential for PB formation, *ZmNAC128* and *ZmNAC130* are  
369 likely to play important roles in PB formation. There were no apparent DAP-seq  
370 peaks in other zein gene promoters, so the expression of other zein genes is possibly  
371 regulated by their co-factors.

### 372 ***ZmNAC128* and *ZmNAC130* directly regulate the expression of multiple** 373 **important starch metabolism genes**

374 Reduced starch content and enrichment of the starch and sucrose metabolism  
375 KEGG pathways among the observed DEGs of *zmnac128 zmnac130* suggest that the  
376 two NACs may directly regulate expression of genes involved in starch metabolism.  
377 We previously found that the expression of multiple important starch metabolism  
378 genes was downregulated in the *nacRNAi*, but only *Bt2* was characterized as the direct  
379 target gene of *ZmNAC128* and *ZmNAC130* (Zhang et al., 2019).

380 To study which starch metabolism genes are the direct targets of *ZmNAC128* and  
381 *ZmNAC130*, we emphasized the commonly downregulated genes in the 16-DAP  
382 endosperms of both *zmnac128 zmnac130* and *nacRNAi* (Table 1). In all seven  
383 downregulated genes in the *nacRNAi* (Zhang et al., 2019), six genes were also  
384 detected to be significantly downregulated in *zmnac128 zmnac130*, including *Bt2*  
385 (*Zm00001eb176800*), *pullulanase-type starch debranching enzyme* (*Zpu1*,  
386 *Zm00001eb088740*), *SSI* (*Zm00001eb376100*), *Sus1* (*Zm00001eb392880*),

387 *granule-bound starch synthase 1* (*GBSS1*, also named *waxy* [*Wx*],  
388 Zm00001eb378140), *starch branching enzyme IIb* (*SBEIIb*, also named *amylose*  
389 *extender1* [*Ae1*], Zm00001eb242610) (Supplemental Dataset S5). *Starch branching*  
390 *enzyme 1* (*SBE1*, Zm00001eb228530) was detected to be transcriptionally  
391 downregulated only in the *nacRNAi* (Zhang et al., 2019), but its encoded protein was  
392 not reduced in *zmnac128 zmnac130* compared to the WT (Figure 4A).

393 Meanwhile, transcriptome analysis of *zmnac128 zmnac130* found that another  
394 two important starch metabolism genes also significantly downregulated, including  
395 *isoamylase-type starch-debranching enzyme1* (*ISA1*, also named *sugary1* [*Su1*],  
396 Zm00001eb242610) and *starch synthase IIa* (*SSIIa*, also named *sugary2* [*Su2*],  
397 Zm00001eb279740) (Supplemental Dataset S5). Therefore, the complete elimination  
398 of *ZmNAC128* and *ZmNAC130* through CRISPR/Cas9-mediated knockout caused the  
399 downregulated expression of more important starch metabolism genes than their  
400 RNAi-mediated knockdown.

401 To detect the effects of *ZmNAC128* and *ZmNAC130* on starch metabolism, we  
402 performed a suite of immunoblotting assays with antibodies against the major starch  
403 metabolism enzyme proteins in 20-DAP endosperms of *zmnac128 zmnac130* and the  
404 WT (Figure 4A). Consistent with the pronounced reduction in *Zpu1* and *Bt2*  
405 transcripts, their corresponding protein accumulation also decreased by nearly 80% in  
406 *zmnac128 zmnac130* compared to the WT. Moreover, the accumulation of four starch  
407 biosynthesis enzymes, including *GBSS1*, *SS1*, *SSIIa*, and *ISA1* decreased by more  
408 than 50% in *zmnac128 zmnac130* compared to the WT. The accumulation of multiple  
409 other enzymes (*AGPase large subunit shrunken2* [*Sh2*], *Sh1*, *SBEIIb*, *SSIII*, *SSV*, and  
410 *ADP-glucose transporter brittle endosperm 1* [*Bt1*]) decreased by 20%–50% in  
411 *zmnac128 zmnac130* compared to the WT. Taken together, these results indicated that  
412 almost all the detected proteins accumulated to lower levels in *zmnac128 zmnac130*  
413 than in the WT. This could be one main cause for the dramatic reduction in starch  
414 content and kernel weight of *zmnac128 zmnac130*.

415 To investigate which genes were directly regulated by *ZmNAC128* and

416 ZmNAC130, we did the DAP-seq and promoter analysis. In these eight  
417 downregulated starch metabolism genes in *zmnac128 zmnac130*, seven genes (*Bt2*,  
418 *Zpu1*, *GBSSI*, *SS1*, *SSIIa*, *Sus1*, and *SBEIIb*) were found to have binding peaks of  
419 ZmNAC128 and ZmNAC130 in their promoters (Table 1). Besides *Bt2* (Figure 2E),  
420 the promoters of another five genes (*Zpu1*, *GBSSI*, *SS1*, *SSIIa*, and *Sus1*) also  
421 contained the conserved cis-element ACGCAA at positions -1, -394/-692, -2,664, -  
422 875/-970, and -1,613/-1,627 upstream from their corresponding TSS, respectively  
423 (Figure 4B). *Sh1*, *Sh2*, *SSIII*, *SSV*, and *Bt1* exhibited reduced protein accumulation  
424 without a corresponding decrease in transcript level. Notably, although the promoters  
425 of four of these genes (*Sh1*, *Sh2*, *SSIII*, and *SSV*) contain the element ACGCAA, no  
426 binding peaks were detected in any of the four promoters (Table 1 and Supplemental  
427 Figure S6).

428 In contrast, despite the absence of the conserved cis-element ACGCAA in the  
429 promoters of *Bt1* and *SBEIIb*, binding peaks were still detected in both promoters  
430 (Table 1), indicating that NACs can bind to these promoters even in the absence of  
431 their canonical target sequence. CHIP-qPCR further verified the binding relationships  
432 of ZmNAC128 and ZmNAC130 for these five promoters of *Zpu1*, *GBSSI*, *SS1*, *SSIIa*,  
433 and *Sus1* (Figure 4C). Finally, DLR assays were performed to detect the  
434 transactivation activities of ZmNAC128 and ZmNAC130 with respect to the five  
435 promoters. LUC activities driven by the four promoters of *Zpu1*, *GBSSI*, *SS1*, and  
436 *SSIIa* were significantly increased by the co-transformation of 35S promoter-driven  
437 ZmNAC128 and ZmNAC130 (Figure 4D). The *Sus1* promoter was slightly  
438 transactivated only by ZmNAC130 but not ZmNAC128. This suggested that although  
439 ZmNAC128 and ZmNAC130 can bind to this promoter, its transactivation potentially  
440 requires the involvement of other TFs. Similarly, the LUC activities driven by these  
441 five promoters were not stronger upon co-expression of ZmNAC128 and ZmNAC130.  
442 Because both the transcript levels and protein accumulation of *Bt2*, *Zpu1*, *GBSSI*, *SS1*,  
443 and *SSIIa* were significantly reduced in *zmnac128 zmnac130*, ZmNAC128 and  
444 ZmNAC130 function as core TFs for starch metabolism through the direct regulation

445 of these starch metabolism genes, i.e., *Bt2*, *Zpu1*, *GBSS1*, *SS1*, *SSIIa*, and *Sus1*.

446 Because carbohydrate-related pathways were generally enriched in DEGs in  
447 *zmnac128 zmnac130*, we also analyzed the expression of genes involved in the three  
448 primary carbohydrate metabolism pathways: the pentose phosphate pathway,  
449 glycolysis, and the tricarboxylic acid cycle. In contrast to the overall downregulated  
450 expression of starch metabolism genes, many genes in these three pathways were  
451 upregulated in *zmnac128 zmnac130* (Supplemental Dataset S5). The upregulated  
452 expression of many genes involved in these three primary carbohydrate metabolism  
453 pathways seems to indicate negative feedback due to a sharp decrease in starch  
454 metabolism in the endosperm of *zmnac128 zmnac130*, but this hypothesis needs to be  
455 investigated.

#### 456 **Regulatory and physical interactions of ZmNAC128 and ZmNAC130 with O2**

457 Among known endosperm filling-related TF genes, *O2*, *ZmNAC128*, and  
458 *ZmNAC130* are the most highly expressed in the filling-stage endosperm (Chen et al.,  
459 2014). Based on the three RNA-seq datasets from the *ZmNAC128* and *ZmNAC130*  
460 knockdown lines and knockout mutants in this study and our previous publication  
461 (Zhang et al., 2019), we observed that the expression of the *O2* gene is consistently  
462 downregulated in *nacRNAi* and *zmnac128 zmnac130* compared to the corresponding  
463 NT and WT, respectively (Supplemental Figure S7). Importantly, only a few DEGs  
464 were shared across studies, one of which was *O2*, making this TF a candidate target  
465 gene of ZmNAC128 and ZmNAC130.

#### 466 **ZmNAC128 and ZmNAC130 directly regulate the expression of O2**

467 To test whether the two NACs regulate the expression of *O2*, we further  
468 measured the transcript level and protein accumulation of *O2* in the endosperms of  
469 *zmnac128 zmnac130* across the entire filling stages from 12- to 28-DAP. RT-qPCR  
470 analysis showed that the transcript levels of *O2* decreased by nearly 50% on average  
471 in the endosperm of *zmnac128 zmnac130* throughout the whole filling stage (Figure  
472 5A). Likewise, the protein accumulation of *O2* significantly decreased by 60%–80%  
473 in endosperms of *zmnac128 zmnac130* throughout the whole filling stage (Figure 5B



474 and Supplemental Figure S8). These findings support a role for ZmNAC128 and  
475 ZmNAC130 in maintaining the high expression of *O2* in the endosperm across the  
476 whole filling stage.

477 To know whether ZmNAC128 and ZmNAC130 directly regulate the expression  
478 of *O2*, we first examined the DAP-seq data. There were apparent peaks corresponding  
479 to regions bound by ZmNAC128 and ZmNAC130 in the *O2* promoter (Figure 5C).  
480 The peak encompassing binding region contains the maize ABSCISIC ACID  
481 INSENSITIVE3 transcription factor 19 (ZmABI19)-binding RY motif (CATGCATG),  
482 the *O2*/*O11*-binding core motif (ACGT), and three candidate  
483 ZmNAC128/130-binding motifs (GTACGT, CTAGCTA, and TTGCTT) (Figure 5C).  
484 To ascertain which candidate motif in the *O2* promoter can be recognized by  
485 ZmNAC128 and ZmNAC130, we conducted an electrophoretic mobility shift assay  
486 (EMSA) involving recombinant His-ZmNAC128 and His-ZmNAC130 and five  
487 biotin-labeled probes covering a 151-bp region from -510 to -360 bp upstream from  
488 the start codon of *O2* gene (Figure 5D). Only the P3 fragment was bound by  
489 ZmNAC128 and ZmNAC130, to form retarded bands in the gel, and ChIP-qPCR also  
490 confirmed this binding relationship (Figure 5E). The binding specificity of  
491 ZmNAC128 and ZmNAC130 was furthermore verified through the addition of 50×  
492 and 200× unlabeled P3 probes in the reactions, which caused a progressive loss of  
493 retarded bands (Supplemental Figure S9).

494 Subsequently, GTACGT in the P3 was subjected to point mutation analysis. Any  
495 point mutation could abolish the binding interaction of ZmNAC128 and ZmNAC130,  
496 confirming GTACGT as an additional cis-element (Figure 5D). Finally, a DLR assay  
497 was conducted to determine the transactivation ability of ZmNAC128 and  
498 ZmNAC130 with respect to the *O2* promoter. Compared to the empty vector control,  
499 LUC activities driven by the *O2* promoter were significantly increased by  
500 ZmNAC128 or ZmNAC130, and the co-expression of the two NACs resulted in a  
501 slightly but significantly stronger transactivation compared to each individual NAC  
502 alone (Figure 5F). These results indicated that these two NACs play crucial roles in

503 directly activating the high expression of *O2*.

#### 504 **Physical interactions of these three TFs**

505 To test the physical interaction between the three TFs, we performed a series of  
506 *in vitro* and *in vivo* protein-protein interaction assays: pull-down, bimolecular  
507 fluorescence complementation (BiFC), luciferase complementation imaging (LCI),  
508 and co-immunoprecipitation (Co-IP) assays. The pull-down assay results showed that  
509 glutathione S-transferase (GST)-tagged *O2* interacts with His-tagged ZmNAC128 but  
510 not ZmNAC130, while GST-tagged ZmNAC130 interacts with His-tagged  
511 ZmNAC128 (Figure 6A). For BiFC and LCI assays, we cloned the coding sequences  
512 of each TF-encoding gene in-frame with the sequence encoding the N-terminal or  
513 C-terminal half of yellow fluorescent protein (YFP) or LUC, after which we  
514 transformed the resulting constructs into *Agrobacterium tumefaciens*  
515 strain GV3101.

516 Unlike for the negative control with no visible signals, we detected YFP signals  
517 and LUC activity in the *Nicotiana benthamiana* leaves co-infiltrated with *ZmNAC128*  
518 and *O2* constructs as well as in those co-infiltrated with the *ZmNAC128* and  
519 *ZmNAC130* constructs (Figure 6B, Supplemental Figure S10 and S11). We also  
520 conducted a Co-IP assay in which we cloned *ZmNAC128* and *ZmNAC130* in-frame  
521 with a sequence encoding 6×Myc, while *O2* and *ZmNAC130* were cloned in-frame  
522 with a 3×Flag sequence, after which each construct was transiently co-infiltrated in *N.*  
523 *benthamiana* leaves. We detected a band of the expected molecular weight for  
524 Myc-ZmNAC128 in the protein extracts immunoprecipitated with anti-Flag  
525 antibodies from leaves co-expressing *Flag-O2* (or *Flag-ZmNAC130*) and  
526 *Myc-ZmNAC128* (Figure 6C). These results demonstrated that ZmNAC128 interacts  
527 with *O2*, ZmNAC130, and itself, while ZmNAC130 interacts with ZmNAC128 and  
528 itself.

#### 529 **Combined effects of ZmNAC128, ZmNAC130, and O2 on the regulation of** 530 **endosperm filling**

531 To investigate the combined effects of the three TFs on the endosperm filling, we

532 generated a triple mutant *zmnac128 zmnac130 o2*. The two loss-of-function mutants  
533 of *O2* were identified by screening an ethyl methanesulfonate (EMS)-mutagenized  
534 B73 library and were backcrossed to B73 for several generations. We named the two  
535 mutant alleles *o2-1*, which has a premature stop codon in the first exon, and *o2-2*,  
536 which has an acceptor splice site mutation between the first intron and the second  
537 exon (Supplemental Figure S12). In this study, *o2-1* was used for crossing with  
538 *zmnac128 zmnac130*.

539 We isolated homozygous mutants for *zmnac128 zmnac130*, *o2*, and *zmnac128*  
540 *zmnac130 o2* from the offspring of the same F<sub>2</sub> cob resulting from the *zmnac128*  
541 *zmnac130* × *o2* cross. The triple mutant *zmnac128 zmnac130 o2* exhibited a more  
542 poorly filled kernel phenotype than did *zmnac128 zmnac130* (Figure 7A). Compared  
543 to that of the NT segregated from *zmnac128 zmnac130* × *o2* cross, the HKWs of  
544 *o2*, *zmnac128 zmnac130*, and *zmnac128 zmnac130 o2* decreased by 26%, 55%, and  
545 73%, respectively (Figure 7B). Compared to the NT, the mature kernels of *zmnac128*  
546 *zmnac130 o2* exhibited an 80% decrease in starch content and a 50% decrease in  
547 protein content (Figure 7C).

548 We further performed RNA-seq analysis of 16-DAP endosperms from *o2*,  
549 *zmnac128 zmnac130*, *zmnac128 zmnac130 o2*, and the NT. Principal component  
550 analysis showed that the transcriptome of *zmnac128 zmnac130 o2* is more similar to  
551 that of *zmnac128 zmnac130* than *o2* (Figure 8A). The number of DEGs was slightly  
552 higher in *zmnac128 zmnac130 o2* than in *zmnac128 zmnac130* but was twofold higher  
553 than in *o2* (Figure 8B). A Venn diagram of the DEGs also illustrated that more than 60%  
554 of all the DEGs were shared between *zmnac128 zmnac130 o2* and *zmnac128*  
555 *zmnac130*, while less than 30% of DEGs were shared between *zmnac128 zmnac130*  
556 *o2* and *o2* (Figure 8C). This suggested that the two NACs have stronger effects on  
557 endosperm filling than *O2*.

558 As these three TFs significantly impacted the transcriptome of filling-stage  
559 endosperms, it is likely that their shared downstream TFs play crucial roles in their  
560 GRN. We first detected their co-transactivation in their own promoters by a group of

561 DLR assays. O2 was previously reported to exhibit auto-transactivation (Lohmer et al.,  
562 1991 and Yang et al., 2022). Our results demonstrated that the O2 promoter exhibited  
563 a stronger transactivation effect in the presence of all three TFs than when they acted  
564 individually, indicating a synergistic effect of their co-expression (Supplemental  
565 Figure S13). Transcriptome analysis indicated that *ZmNAC130* but not *ZmNAC128* is  
566 significantly downregulated in the *o2* mutant (Supplemental Figure S14A). DLR  
567 results revealed that O2 can transactivate the promoter of *ZmNAC130*, but not that of  
568 *ZmNAC128*, which is consistent with their respective expression patterns in *o2*  
569 (Supplemental Figure S14B).

570 Similar to the O2 promoter, the promoters of *ZmNAC130* and *ZmNAC128* were  
571 found to be strongly activated by the co-expression of all three TFs (Supplemental  
572 Figure S14B). In addition, several TFs have been reported as the direct downstream  
573 genes of O2, including *bZIP G-box binding factor 1 (GBP1)*, *MYBR13*, *bZIP17*, and  
574 *NKD2* (Li et al., 2015 and Zhan et al., 2018). To detect which ones can also be the  
575 target genes of *ZmNAC130* and *ZmNAC128*, we analyzed binding peaks of  
576 *ZmNAC128* and *ZmNAC130* in these four gene promoters. Only the *MYBR13*  
577 promoter was apparently bound by both *ZmNAC128* and *ZmNAC130* (Supplemental  
578 Figure S15A). DLR results indicated that all three TFs were capable of individually  
579 transactivating the *MYBR13* promoter, with the highest LUC activity observed in the  
580 co-expression of the three TFs (Supplemental Figure S15B). Consistent with the  
581 promoter transactivation, the expression of *MYBR13* was the lowest in *zmnac128*  
582 *zmnac130 o2* (Supplemental Figure S15C), hinting at their synergistic regulation.

### 583 **Combined effects of the three TFs on the regulation of zein synthesis**

584 GO term enrichment analysis of the 581 DEGs common among the three mutants  
585 revealed that “nutrient reservoir activity” (GO: 0045735, *p*-value = 1.8E–18) was the  
586 most significantly enriched GO term (Supplemental Figure S16). This is consistent  
587 with the strong influence of O2, *ZmNAC128*, and *ZmNAC130* on the expression of  
588 zein family genes. The expression of all zein genes was lower in *zmnac128 zmnac130*  
589 *o2* than in *zmnac128 zmnac130* or *o2* (Supplemental Dataset S6). Except for 27-kD

590  $\gamma$ -zein, most zein proteins were barely visible, as shown by Coomassie Brilliant Blue  
591 staining (Figure 8D). In view of the transactivation of O2 on the promoters of 27-kD  
592  $\gamma$ -zein and 50-kD  $\gamma$ -zein, our further detection indicated that ZmNAC128 and  
593 ZmNAC130 can coordinate with O2 to enhance the transactivation of the promoter of  
594 50-kD  $\gamma$ -zein but not that of 27-kD  $\gamma$ -zein (Supplemental Figure S17). Therefore, the  
595 synergistic effect of these three TFs on the expression of most zein genes seems  
596 similar to that of O2, PBF1, and OHPs, which do not involve direct transcriptional  
597 regulation (Zhang et al., 2015).

### 598 **Combined effects of the three TFs on the regulation of starch synthesis**

599 Consistent with the dramatic reduction in starch contents in mature *zmnac128*  
600 *zmnac130 o2* kernels, starch accumulation decreased in the filling-stage endosperms  
601 of *zmnac128 zmnac130 o2* compared to *zmnac128 zmnac130* and *o2*, as evidenced by  
602 potassium iodide staining (Supplemental Figure S18). However, the expression of  
603 most starch metabolism genes and other carbohydrate metabolism genes was  
604 downregulated to a similar extent in *zmnac128 zmnac130 o2*, *zmnac128 zmnac130*,  
605 and *o2* (Supplemental Dataset S7). We further performed the immunoblotting assay to  
606 detect the protein accumulation of starch metabolism enzymes in 20-DAP endosperms  
607 from NT, *o2*, *zmnac128 zmnac130*, and *zmnac128 zmnac130 o2*. Consistent to the  
608 previous findings that O2 directly regulates the expression of *SSIII* and *PPDK* (Zhang  
609 et al., 2016), these two proteins and *SSV* were reduced in both *o2* and *zmnac128*  
610 *zmnac130 o2* (Figure 8E). *Zpu1*, *GBSS1*, *SS1*, *Bt2*, and *SSIIa* were reduced in both  
611 *zmnac128 zmnac130* and *zmnac128 zmnac130 o2* (Figure 8E). The protein  
612 accumulation of more starch metabolism enzymes was lower in *zmnac128 zmnac130*  
613 *o2* than in *zmnac128 zmnac130* or *o2*. Therefore, the two NACs and O2 separately  
614 regulated the expression of different starch metabolism genes. This could be one  
615 major cause for the relatively low amount of starch metabolism in *zmnac128*  
616 *zmnac130 o2*.

617 **Regulation of sugar and nutrient transport from maternal to filial tissue:**  
618 **ZmNAC128, ZmNAC130, and O2 regulate the expression of key transporter**

619 **genes in the BETL**

620 Our RNA *in situ* hybridization results showed that *ZmNAC128* and *ZmNAC130*  
621 are expressed not only in the SE but also in the BETL (Figure 9A). This suggested  
622 that the two NACs possibly regulate the expression of nutrient transfer-related genes  
623 in the BETL. To date, two sugar transporters (*ZmSWEET4c* and *ZmSUGCAR1*,  
624 which are also responsible for K<sup>+</sup> uptake), one cell wall invertase (*ZmMN1*), and one  
625 zinc transporter (*ZmYSL2*) have been characterized as playing crucial roles in  
626 mother-to-endosperm transport in the BETL (Chao et al., 2022; Cheng et al., 1996;  
627 Guan et al., 2020; He et al., 2021; Sosso et al., 2015; Wei et al., 2021; Yang et al.,  
628 2022a; Zhou et al., 2021).

629 Transcriptome analysis of the whole 16-DAP endosperms, including the BETL,  
630 revealed that the expression of *ZmSWEET4c*, *ZmSUGCAR1*, *ZmYSL2*, and *ZmMN1*  
631 was significantly reduced by 8.7-, 7.2-, 6.2-, and 4.8-fold in *zmnac128 zmnac130*  
632 compared to the WT, respectively (Figure 9B). DAP-seq analysis indicated that there  
633 are peaks corresponding to regions bound by *ZmNAC128* and *ZmNAC130* in the  
634 promoters of *ZmSWEET4c* and *ZmSUGCAR1*, but not in the promoters of *ZmMN1* and  
635 *ZmYSL2* (Figure 9C). We further found the cis-element GTACGT consistently around  
636 the peak binding regions in the *ZmSWEET4c* and *ZmSUGCAR1* promoters (Figure  
637 9C). The CHIP-qPCR results confirmed the binding of *ZmNAC128* and *ZmNAC130*  
638 to the two promoters (Figure 9D). We found three GTACGT motifs in the  
639 *ZmSUGCAR1* promoter, whereas *ZmNAC128* and *ZmNAC130* recognized only the  
640 second motif-containing region (Figure 9D).

641 Typically, the protein-DNA interactions could be disrupted by the flanking DNA  
642 sequence around the binding motif. For instance, there are two ACGCAA elements  
643 within a 1,000 bp region of the *Bt2* promoter upstream from the start codon, but  
644 *ZmNAC128* and *ZmNAC130* recognize only the one near the start codon (Zhang et  
645 al., 2019). Although our DAP-seq analysis did not find the peaks bound by  
646 *ZmNAC128* and *ZmNAC130* in the *ZmYSL2* promoter, CHIP-qPCR showed the  
647 interaction of *ZmNAC128* and *ZmNAC130* with the GTACGT-centered fragment in

648 the *ZmYSL2* promoter (Figure 9D). This result suggested that our DAP-seq might  
649 have missed some targets. We finally performed DLR assays to detect the  
650 transactivation of *ZmNAC128* and *ZmNAC130* on these four promoters. Indeed,  
651 *ZmNAC128* or *ZmNAC130* significantly enhanced the LUC activities driven by the  
652 promoters of *ZmSWEET4c*, *ZmSUGCAR1*, and *ZmYSL2* but not by the *ZmMN1*  
653 promoter, while their LUC activities were not higher upon co-expression of  
654 *ZmNAC128* and *ZmNAC130* (Figure 9E).

655 In view of the more severe endosperm-filling defect of *zmnac128 zmnac130 o2*,  
656 we also investigated whether *O2* is involved in the regulation of the four genes  
657 (*ZmSWEET4c*, *ZmSUGCAR1*, *ZmYSL2*, and *ZmMN1*). Transcriptome analysis showed  
658 that the expression of only *ZmYSL2* was significantly downregulated by twofold in *o2*,  
659 although the expression of all four genes was downregulated in *zmnac128 zmnac130*  
660 *o2* (Supplemental Figure S19A). DLR results indicated that *O2* could enhance LUC  
661 activities driven by the promoters of *ZmSWEET4c* and *ZmSUGCAR1*. Meanwhile,  
662 *ZmNAC128* and *ZmNAC130* together with *O2* could further enhance the  
663 transactivation activities driven by the promoters of *ZmSWEET4c*, *ZmSUGCAR1*, and  
664 *ZmYSL2* (Supplemental Figure S19B). Taken together, these results suggested that *O2*  
665 and the two NACs synergistically co-activate these three transporter-encoding genes.

#### 666 **Combined effects of these three TFs on sugar and nutrient uptake**

667 To detect whether the mutations of the three core TFs affect kernel nutrient  
668 uptake, we measured the contents of soluble sugars and elements transported by  
669 *ZmSWEET4c*, *ZmSUGCAR1*, and *ZmYSL2* in the mature dry kernels of the NT, *o2*,  
670 *zmnac128 zmnac130*, and *zmnac128 zmnac130 o2*. The levels of soluble sugars  
671 (glucose, fructose, and sucrose) in the kernels could be affected by multiple factors,  
672 including BETL-related uptake ability and carbohydrate metabolism and  
673 accumulation. The levels of glucose, fructose, and sucrose were significantly  
674 increased in the kernels of *o2* compared to the NT (Figure 10A). These results are  
675 consistent with those corresponding to the previous determination of soluble sugars in  
676 *o2* kernels (Zhang et al., 2016), which is related to decreased starch biosynthesis.

677 However, although starch accumulation is lower in *zmnac128 zmnac130* than *o2*, the  
678 levels of soluble sugars are also lower in *zmnac128 zmnac130*.

679 In particular, the sucrose level is significantly decreased in *zmnac128 zmnac130*  
680 compared to the NT, which is similar to the effects that occur when *ZmSUGCAR1* is  
681 mutated (Yang et al., 2022). Conversely, the levels of these three soluble sugars are  
682 much higher in *zmnac128 zmnac130 o2* than *zmnac128 zmnac130* and *o2*, which is  
683 similar to what occurs in mutants due to the blockage of starch biosynthesis. This  
684 reflects the importance of the three core filling TFs in starch synthesis. Although the  
685 evaluation of sugar uptake is relatively complex, the loss-of-function mutations of  
686 *ZmNAC128* and *ZmNAC130* indeed affect kernel sugar uptake, especially for sucrose.

687 *ZmSUGCAR1* and *ZmYSL2* can transport K and Zn from maternal to  
688 endosperm respectively, so element analysis was also performed on the mutant  
689 kernels. Although there was no statistically significant change in the K level between  
690 *zmnac128 zmnac130* and the NT, a significant reduction in the K level was observed  
691 in *zmnac128 zmnac130* compared to *o2*.(Figure 10A). The mutation of *ZmNAC128*  
692 and *ZmNAC130* affects the expression of *ZmSUGCAR1* and in turn its transport  
693 ability for K and sucrose. The level of Zn, but not Fe, is significantly decreased in  
694 *zmnac128 zmnac130* compared to the NT and *o2*. This is consistent with the fact that  
695 *ZmYSL2* is responsible for the uptake of Zn rather than Fe (Chao et al., 2022), while  
696 the Zn level was observed to be even lower in *zmnac128 zmnac130 o2* than *zmnac128*  
697 *zmnac130* (Figure 10A).

698 Overall, *O2*, *ZmNAC128*, and *ZmNAC130* affect the uptake of soluble sugars,  
699 Zn, and K potentially partly through the regulation of the expression of *ZmSWEET4c*,  
700 *ZmSUGCAR1*, and *ZmYSL2* (Figure 10B). By itself, *O2* seems to have a very weak  
701 effect on the uptake of these nutrients, but it can enhance the function together with  
702 *ZmNAC128* and *ZmNAC130* to affect the transport abilities of *ZmSWEET4c*,  
703 *ZmSUGCAR1*, and *ZmYSL2*.

704

705 **Discussion**



706 **The molecular basis of the genetic redundancy between *ZmNAC128* and**  
707 ***ZmNAC130***

708 *ZmNAC128* and *ZmNAC130* are a pair of duplicated genes that arose from the  
709 allotetraploidization of maize (Zhang et al., 2019). The previous study suggested the  
710 functional redundancy of *ZmNAC128* and *ZmNAC130* because they regulate the  
711 expression of the same downstream genes (*16-kD  $\gamma$ -zein* and *Bt2*) by recognizing a  
712 common binding motif ACGCAA (Zhang et al., 2019). This study demonstrated the  
713 genetic redundancy of *ZmNAC128* and *ZmNAC130* by generating their knockout  
714 mutations. It is generally accepted that the two copies of duplicated genes can be  
715 retained by functional divergence or stronger functions (such as robustness) in the  
716 evolution (Huang et al., 2023). Undoubtedly, *ZmNAC128* and *ZmNAC130*  
717 commonly exert stronger functions in endosperm filling.

718 *ZmNAC128* and *ZmNAC130* shared high sequence similarities in both NAC and  
719 transactivation domains (Zhang et al., 2019), hinting at their similarities in structure  
720 and function. Indeed, the single mutations of *ZmNAC128* and *ZmNAC130* have little  
721 effect on the transcriptome (such as few DEGs) of filling endosperm, but their double  
722 mutant leads to thousands of DEGs. Protein-protein interaction experiments also  
723 indicated that these two NACs can form homo- or hetero-dimer. So when one NAC is  
724 absent, the other NAC can form a homodimer to function in filling endosperms. DLR  
725 assays were used to assess which kind of interaction exerts stronger functions, either  
726 homo- or hetero-dimerization. With the addition of *16-kD  $\gamma$ -zein* and *Bt2* (Zhang et al.,  
727 2019), the total fourteen direct downstream genes of *ZmNAC128* and *ZmNAC130*  
728 have been verified by their promoter transactivation. In general, the co-expression of  
729 *ZmNAC128* and *ZmNAC130* does not have stronger transactivation in many of these  
730 promoters than either of them alone, indicating that the two kinds of dimers have  
731 roughly equivalent abilities to activate the expression of their target genes.

732 On the other hand, although the single mutants *zmnac128* and *zmnac130* have no  
733 visible kernel phenotypes, their kernel starch contents are slightly reduced compared  
734 to the WT. It suggests that the absence of one NAC seems to have a weak effect on

735 their dimerization or polymerization in endosperm cells. Indeed, the co-expression of  
736 O2, ZmNAC128, and ZmNAC130 exhibited the highest transactivation activities on  
737 the promoters of many of their common target genes in all combinations. And  
738 according to the interaction of O2, ZmNAC128, and ZmNAC130, it is supported that  
739 ZmNAC128 and ZmNAC130 should form a heterodimer and interact with other  
740 co-factors (such as O2) to more effectively regulate complex endosperm filling  
741 (Figure 10B).

### 742 **O2, ZmNAC128, and ZmNAC130 coordinate the synchronized biosynthesis of** 743 **zeins and starch**

744 The regulation of zein gene expression during endosperm filling has been  
745 comprehensively investigated (Dai et al., 2021; Yang et al., 2023). This study further  
746 broadens the understanding of the transcriptional regulation of zein gene expression.  
747 Unlike other TFs regulating the expression of zein genes, ZmNAC128 and  
748 ZmNAC130 specifically regulate the expression of all three (*16-*, *27-*, and *50-kD*)  
749  $\gamma$ -zein genes and mediate the expression of other zein genes. However, with the  
750 exception of that of 16-kD  $\gamma$ -zein, the accumulation of other zein proteins is not  
751 apparently reduced in *zmnac128 zmnac130*. This is very similar to the regulatory  
752 ability of O2 on the expression of zein family genes. Although O2 regulates the  
753 expression of most zein genes (excluding *16-kD*  $\gamma$ -zein) (Li et al., 2015; Zhan et al.,  
754 2018), the accumulation of only  $\alpha$ -zeins is apparently reduced in *o2*. The two NACs  
755 and O2 are the major regulators of the expression of *16-kD*  $\gamma$ -zein and  $\alpha$ -zein,  
756 respectively, while they have minor effects on the regulation of other zein gene  
757 expression.

758 Although the protein accumulation of O2 is largely reduced in *zmnac128*  
759 *zmnac130*,  $\alpha$ -zein accumulation is not apparently reduced in this mutant. This  
760 suggested that partial expression of O2 is sufficient to activate the expression of  
761  $\alpha$ -zein genes, while other TFs also possibly compensate for the reduction of O2 in  
762 *zmnac128 zmnac130*. In addition, all three TFs can transactivate the expression of the  
763 *27-kD*  $\gamma$ -zein gene, although the accumulation of the 27-kD  $\gamma$ -zein protein is not

764 apparently reduced in the triple mutant. Indeed, multiple TFs have been characterized  
765 to regulate the expression of 27-kD  $\gamma$ -zein (Li et al., 2015; Li et al., 2018; Pysh et al.,  
766 1993; VicenteCarbajosa et al., 1997; Wu and Messing, 2012; Zhang et al., 2015),  
767 supporting the idea that 27-kD  $\gamma$ -zein is essential for PB formation and endosperm  
768 filling. The other TFs thus could compensate for the absence of *O2*, *ZmNAC128*, and  
769 *ZmNAC130*. Nevertheless, most zein proteins are almost undetectable in *zmnac128*  
770 *zmnac130 o2*, demonstrating the core function of these three TFs in the regulation of  
771 zein synthesis.

772 Moreover, *ZmNAC128* and *ZmNAC130* directly regulated the expression of at  
773 least six important starch metabolism genes. The transcript and protein levels of other  
774 major starch metabolism genes were also reduced to varying degrees in *zmnac128*  
775 *zmnac130*, indicating that *ZmNAC128* and *ZmNAC130* are critical TFs for starch  
776 metabolism. *ZmNAC128* and *ZmNAC130* play even more important roles than *O2* in  
777 the synchronized biosynthesis of zein and starch. In agreement with this notion,  
778 compared with *zmnac128 zmnac130*, *zmnac128 zmnac130 o2* showed less  
779 accumulation of storage reserves and more poorly filled kernels. Moreover, these  
780 three TFs have no universally synergistic effect on the expression of their common  
781 target genes for the biosynthesis of starch and zeins. Perhaps the accumulation of the  
782 two major storage components in the endosperm is synergistically regulated through a  
783 more complex mechanism by the three core TFs, as they modulate the expression of  
784 hundreds or thousands of genes, thus imposing hierarchical regulation on other  
785 aspects of development.

### 786 **Regulatory mechanism underlying the high expression of *O2*, *ZmNAC128*, and** 787 ***ZmNAC130* during the endosperm-filling stage**

788 Although *O2* is a well-known core TF in filling endosperm, the mechanism of  
789 regulating *O2* expression is rather unclear. Two recent studies demonstrated that  
790 *ZmABI19* and *ZmbZIP29* are highly expressed in the early stage of kernel  
791 development and play initial roles in grain filling (Yang et al., 2021; Yang et al.,  
792 2022b). *ZmABI19* initiates the expression of *O2* and *ZmNAC130*, while *ZmbZIP29*

793 and *ZmABI19* synergistically transactivate the expression of *O2* upon abscisic acid  
794 treatment. Because *ZmABI19* and *ZmbZIP29* are expressed during the early stage,  
795 they function mainly as initial regulators of *O2* expression. Auto-activation of *O2* may  
796 play a role in activating its expression during the filling stage (Lohmer et al., 1991;  
797 Yang et al., 2021), but it is difficult to quantify this contribution. This investigation  
798 illustrated how *ZmNAC128* and *ZmNAC130* act as major regulators to control the  
799 expression of more than 50% of transcripts and proteins of *O2* across the entire filling  
800 stage via direct regulation. Moreover, the transactivation activity of *O2* can be further  
801 enhanced in the presence of both NACs and *O2*. Therefore, these three TFs clearly  
802 play a decisive role in regulating the high expression of *O2* in the endosperm  
803 throughout the whole filling stage.

804 According to this investigation, although *O2* also regulates the expression of  
805 *ZmNAC130*, it does not appear to be the core regulator for the expression of  
806 *ZmNAC128* and *ZmNAC130*. Because the contribution of auto-activation is hard to  
807 quantify with respect to the expression of *ZmNAC128* and *ZmNAC130*, their high  
808 expression in filling endosperm needs to be further investigated. Nevertheless, a  
809 hierarchical regulatory circuit among these three core TFs is a prerequisite for  
810 activating their high expression and endosperm filling.

### 811 **The function of putative orthologs of *ZmNAC128* and *ZmNAC130* in the grains** 812 **of other species**

813 Grain filling involves two synchronized processes, i.e., maternal-to-filial nutrient  
814 transport and storage component synthesis. However, it was previously unknown  
815 whether the expression of the genes involved in these two distinct processes is  
816 coordinated by common TFs. Recent advances in the functional genomics of maize  
817 kernels prompted us to investigate the link between nutrient uptake and storage  
818 reserve synthesis. For instance, the maize nutrient uptake-related genes *ZmSWEET4c*,  
819 *ZmSUGCARI*, and *ZmYSL2* are partly or specifically expressed in the filling  
820 endosperm, which is highly consistent with the expression pattern of genes  
821 responsible for the synthesis of starch and zeins. Here, we found that *ZmNAC128* and

822 ZmNAC130 regulate the expression of important filling-related genes in both the  
823 BETL and the SE, which in turn facilitate nutrient uptake and storage reserve  
824 synthesis in the endosperm (Figure 10B).

825 There are no reports on the mechanism underlying the coordination of  
826 mother-to-endosperm nutrient transfer and storage reserve biosynthesis during grain  
827 filling in other cereals, such as rice (*Oryza sativa*) and wheat (*Triticum aestivum*).  
828 OsNAC20, OsNAC26, and TaNAC019, which are homologous to ZmNAC128 and  
829 ZmNAC130, were recently shown to coordinate the biosynthesis of starch and storage  
830 proteins in the endosperm (Liu et al., 2020; Wang et al., 2020; Gao et al., 2021),  
831 although it has yet to be tested whether they are involved in nutrient uptake. Based on  
832 DEG analysis of *OsNAC20*, *OsNAC26*, and *TaNAC019* mutants (Supplemental Figure  
833 S20), we preliminarily found that the expression of TraesCS6D02G012100 (a  
834 homolog of *ZmSWEET4c*) (Sosso et al., 2015) and TraesCSU02G13020 (a homolog  
835 of *ZmSUGCARI*) (Yang et al., 2022a) is significantly downregulated in the  
836 *TaNAC019* mutant.

837 Like maize, wheat also has a typical transfer cell layer that mediates nutrient  
838 transfer from the mother plant to the grain. We hypothesize that TaNAC019 might  
839 also be involved in the regulation of endosperm nutrient uptake, although this  
840 hypothesis needs to be investigated. However, *OsSWEET4c*, *OsNPF7.9*, and *GRAIN*  
841 *INCOMPLETE FILLING1 (GIF1)* (Wang et al., 2008) were not among the DEGs  
842 identified in the double mutant for *OsNAC20* and *OsNAC26*, indicating that their  
843 expression is not significantly altered in the mutant. This suggested that OsNAC20  
844 and OsNAC26 are unlikely to be involved in the regulation of nutrient uptake, but this  
845 hypothesis also needs to be investigated.

846 In summary, ZmNAC128 and ZmNAC130 coordinate with O2 to promote  
847 endosperm filling, from nutrient uptake in the BETL to the synthesis of starch and  
848 zeins in the SE, while regulate their own expression (Figure 10B). Therefore, our  
849 findings greatly broaden our understanding of grain filling and have potential  
850 importance for improving grain-filling efficiency in breeding.

851

## 852 **Materials and methods**

### 853 **Plant materials and growth conditions**

854 The CRISPR/Cas9-mediated knockout lines of *ZmNAC128* and *ZmNAC130* were  
855 generated in the maize (*Zea mays*) KN5585 background by *Agrobacterium*  
856 (*Agrobacterium tumefaciens*)-mediated transformation as previously described (Frame  
857 et al., 2011). The T<sub>1</sub> plants were backcrossed to KN5585 and then self-pollinated to  
858 produce homozygous knockout lines without the CRISPR/Cas9 cassette, as  
859 determined by PCR identification. The two loss-of-function mutant lines for *O2* were  
860 identified from an EMS-mutagenized maize inbred B73 population. *o2-1* harbors a  
861 premature termination codon at the +417 position downstream from the first codon  
862 ATG. *o2-2* is an acceptor splice site mutation at the boundary between the first intron  
863 and the second exon. The *o2-1* mutant used in this study was backcrossed twice to the  
864 WT B73 and self-pollinated several times. The triple mutant *zmnac128 zmnac130 o2*  
865 was generated from an F<sub>2</sub> ear of *zmnac128 zmnac130 ×o2-1*. The other three  
866 genotypes, NT, *o2*, and *zmnac128 zmnac130*, were also identified from the same F<sub>2</sub>  
867 ear. For the transgenic materials of the 27-kD  $\gamma$ -zein promoter-driving *ZmNAC128* or  
868 *ZmNAC130* expression, the 3' terminus for each gene was linked to a short nucleotide  
869 sequence encoding the 3×FLAG tag. The expression cassettes were transformed into  
870 the modified binary vector pTF102 with the GFP driven by the 10-kD  $\delta$ -zein promoter  
871 as the visible selection marker (Wu and Messing, 2012). The transgenic lines were  
872 also generated in the KN5585 background through *Agrobacterium*-mediated  
873 transformation. All maize materials were planted in the field of Hefei (Anhui Province,  
874 China) and Sanya (Hainan Province, China). *Nicotiana benthamiana* plants were  
875 cultivated in a chamber maintained at a constant temperature of 21°C. The humidity  
876 level inside the chamber was maintained at 50%-60%, and the plants were exposed to  
877 a 16-hour light cycle each day. The primers for construction and genotyping are listed  
878 in Supplemental Dataset S8.

### 879 **Prediction of starch and protein content in the mature kernels**

880 Mature dry kernels were milled into flour and then filtered with a 50-mesh  
881 stainless steel screen. The starch and protein content of the milled flour was predicted  
882 using a pre-constructed calibration model based on MPA-type Fourier transform  
883 near-infrared spectrophotometer (Bruker, Germany). The model calibration was based  
884 on 30 different varieties of maize flour samples, of which starch and protein content  
885 were determined by the Amyloglucosidase- $\alpha$ -Amylase Method (AOAC 996.11) and  
886 the Kjeldahl method (Lynch and Barbano, 1999), respectively. These sample spectra  
887 were collected on the MPA spectrophotometer and the modeling algorithm was partial  
888 least squares regression. The coefficient of determination ( $R^2$ ) of starch and protein  
889 models were 0.826 and 0.984, respectively, and root-mean-square error of  
890 cross-validation (RMSECV) values were 0.533 and 0.123, respectively. The mature  
891 kernel flour of each material was divided into four portions for measurement. To  
892 calculate the percentage of starch and protein in a single kernel per genotype, the  
893 values were further calculated based on the kernel weight.

#### 894 **Determination of soluble sugars in the mature kernels**

895 The determinations were performed according to the methods as previously  
896 reported (Deng et al., 2020). 50 mg of different fresh or matured maize endosperm  
897 powder were extracted with 2 mL of deionized water. After incubating the tubes for  
898 30 min on ice, the supernatants were moved to a new 2 mL centrifuge tube after  
899 centrifugation at 13,000 g for 15 min at 4 °C and then filtered with the 0.22  $\mu$ m filter.  
900 The resulting filtered liquid was diluted tenfold with deionized water for measurement.  
901 The determinations were performed on the ion chromatography (ICS5000, Thermo  
902 Fisher Scientific) using a CarboPac PA-20 column (Nagamine and Komae, 1996). The  
903 mobile phase consisted of solvent A (deionized water) and solvent B (200 mM  
904 NaOH).

#### 905 **Iodine staining starch in the developing endosperm**

906 The 16- and 20-DAP fresh kernels were longitudinally cut in half with a  
907 single-edge blade and the cut kernels were placed in the iodine solution (0.3 g of  $I_2$   
908 and 2 g of KI in 100 ml of deionized water in an amber glass bottle to protect from

909 light at room temperature) for 3 min. Immediately, the staining kernels were rinsed  
910 with deionized twice, and then observed and photographed under a stereomicroscope  
911 (LEICA S9i).

### 912 **RNA *in situ* hybridization**

913 The 12-DAP B73 kernels were used for RNA *in situ* hybridization. cDNA  
914 fragments of *ZmNAC128* and *ZmNAC130* were amplified, and their antisense and  
915 sense RNA probes were synthesized by *in vitro* transcription using T7 RNA  
916 polymerase with DIG RNA Labeling Mixture (Roche). Tissue processing and *in situ*  
917 hybridization experiments using 10- $\mu$ m sections were performed according to the  
918 methods described previously (Zhang et al., 2015). A light microscope (Leica DM500)  
919 was used to observe paraffin-embedded sections of filling-stage kernels.

### 920 **Element profiling**

921 The elemental analysis was conducted by inductively coupled plasma mass  
922 spectrometry (ICP-MS) as previously described (Chao et al, 2022). This analysis was  
923 conducted in the mature kernels of *o2*, *zmnac128 zmnac130*, and *zmnac128 zmnac130*  
924 *o2* as well as the corresponding wild type. Six dry mature kernels of each genotype  
925 were ground into powder by a tomized grinder with a grinding tank (material:  
926 polytetrafluoroethylene) and beads (material: Jargonite) manufactured by Jingxin  
927 Industry Co., Ltd., Shanghai. 2-5 mg of each sample was used for ICP-MS analysis.  
928 The elemental content by ICP-MS was measured following the method as previously  
929 described (Chao et al, 2022) and all the solid samples were normalized with a  
930 heuristic algorithm using the best-measured elements as previously described (Lahner  
931 et al, 2003).

### 932 **Electron- and light-microscope observation**

933 To observe endosperm texture and starch granules of the wild type and mutants,  
934 mature kernels were placed in a drying oven at 45°C for at least 24 h and then cut  
935 along the longitudinal axis of the kernel. Subsequently, the endosperm texture and  
936 starch granules in the longitudinal section were observed under a scanning electron  
937 microscope (ZEISS Gemini SEM 500), following the instructions outlined on the



938 ZEISS Microscopy website (<https://www.zeiss.com/microscopy/en/home.html>). For  
939 kernel phenotype observations, the longitudinal sections of kernels were observed  
940 under a stereomicroscope (LEICA S9i).

#### 941 **Protein extraction, polyclonal antibody generation, and immunoblotting assay**

942 Zein and non-zein proteins from endosperm and kernels were extracted as described  
943 previously (Zhang et al., 2015). The protein concentration was determined with a  
944 Compat-Able Protein Assay Preparation Reagent Kit and a BCA Protein Assay Kit  
945 (Pierce) according to the standard procedures. 10 µg of non-zein proteins in each  
946 sample was loaded for immunoblotting assays with the corresponding antibodies as  
947 described previously (Zhang et al., 2015). The antibody against O2 protein was  
948 previously generated (Yang et al., 2021). For the production of antibodies against  
949 starch metabolism enzymes in this study, their partial cDNAs (encoding 60-200 amino  
950 acids) were amplified by PCR and cloned into the pET51b expression vector. The  
951 recombinant plasmids were transformed into *Escherichia coli* BL21 Rosetta 2 (DE3)  
952 competent cells. Bacteria were grown at 37 °C until the absorbance at 600 nm  
953 (OD600) reached 0.6. Protein production was induced with 0.1 mM isopropyl  
954 β-d-1-thiogalactopyranoside (IPTG). Bacteria were cultured at 37 °C for an additional  
955 5 h before pelleting by centrifugation at 4,000 g. The fusion protein was purified on a  
956 Ni-NTA His Bind Resin (Novagen). The eluted proteins were dialyzed in PBS five  
957 times, and about 6 mg was sent to Shanghai Orizymes Biotech Company to produce  
958 the antibodies. Detailed information on antigens and their efficacy and specificity are  
959 in Supplemental Figure S21 and Supplemental Table S2.

#### 960 **Protein purification, pull-down, and Co-IP assay**

961 For the pull-down assay, O2 and ZmNAC130 were fused to a GST tag, and  
962 ZmNAC128 and ZmNAC130 were fused to a His-TF tag. The encoding plasmids  
963 were transformed into *E. coli* Rosetta, and recombinant proteins were extracted and  
964 purified. GST, GST-ZmNAC128, and GST-ZmNAC130 were incubated with  
965 glutathione beads (GE Healthcare) at 4°C for 2–3 h; the beads were incubated with  
966 His-ZmNAC128 and His-ZmNAC130 at 4°C for 2 h. After washing and elution, the

967 proteins were separated by SDS-PAGE and subjected to immunoblot analysis with  
968 anti-GST (ProteinTech, No. 10000-0-AP, 1:5,000), anti-His (TransGen Biotech,  
969 HT501, 1:5,000), and anti-NAC (Shanghai Orizymes Biotech Company, PAB191213,  
970 1:5,000).

971 For the Co-IP assay, O2 and ZmNAC130 were fused to 3xFlag, and ZmNAC128  
972 and ZmNAC130 were fused to a 6xMyc tag. The encoding plasmids were transformed  
973 into *Agrobacterium* strain GV3101 and co-expressed in *Nicotiana benthamiana* leaves.  
974 Total proteins were extracted in IP buffer (150 mM NaCl, 12.7 mM KCl, 25 mM  
975 Na<sub>2</sub>HPO<sub>4</sub>, .5 mM KH<sub>2</sub>PO<sub>4</sub>, 1, 10% [v/v] glycerol, 0.01 mM EDTA, 0.05% [v/v] NP-40,  
976 1 mM PMSF, 5 mM DTT, and 1× protease inhibitor cocktail) at 4°C for 1 h and then  
977 incubated with Flag beads (Sigma–Aldrich, M8823-1 mL) at 4°C for 2–3 h. The beads  
978 were washed three to four times with washing buffer (50 mM Tris-HCl, pH 7.4, 150  
979 mM NaCl, and 0.1% [v/v] NP-40). After washing, the eluted proteins were separated  
980 by SDS-PAGE and subjected to immunoblot analysis with anti-Myc (Cell Signaling  
981 Technology, 2278S, 1:2,000) and anti-Flag (Sigma–Aldrich, F1804, 1:2,000)  
982 antibodies. The above protein bands were visualized using a Tanon-5200M imaging  
983 system. The primers are listed in Supplemental Dataset S8.

#### 984 **BiFC and LCI assays**

985 O2, ZmNAC128, and ZmNAC130 were fused with the N-terminal or C-terminal  
986 half of YFP or luciferase (LUC). The encoding plasmids were transformed into  
987 *Agrobacterium* strain GV3101 and then co-expressed in *N. benthamiana* leaves. YFP  
988 fluorescence was visualized using confocal microscopy (ZEISS980; Carl Zeiss). YFP  
989 signals were excited at 514 nm, and emission was detected in the range of 520-545  
990 nm with an intensity value of approximately 0.5% and a gain value of around 600. For  
991 LCI assays, leaf samples were infiltrated with 1× luciferin, and luciferase signals  
992 were detected using a Tanon-5200M imaging system. The primers are listed in  
993 Supplemental Dataset S8.

#### 994 **RNA extraction and reverse transcription quantitative PCR**

995 Total RNA was extracted from 12-, 16-, 20-, 24-, and 28-DAP endosperm using

996 TRIzol reagent (Invitrogen) and purified with an RNeasy Mini Kit after DNase I  
997 digestion (Qiagen). First-strand cDNA was then generated with a SuperScript III First  
998 Strand Kit (Invitrogen). RT-qPCR was performed with SYBR Green (Takara) on a  
999 CFX Connect Real-Time PCR system (Bio-Rad) according to the standard operating  
1000 manual. The comparative CT ( $\Delta\Delta CT$ ) method was employed for the relative  
1001 quantification of gene expression (Livak and Schmittgen, 2001), with *ACTIN* serving  
1002 as the reference. The primers are listed in Supplemental Dataset S8.

### 1003 **RNA-seq**

1004 The details for RNA-seq were as described previously. Total RNA was extracted  
1005 from 16-DAP maize kernel endosperm using TRIzol reagent (Invitrogen) according to  
1006 the manufacturer's instructions. The concentration and quality of total RNA (from  
1007 two or three independent groups of endosperms for each genotype) were determined  
1008 on a NanoDrop™ 2000/2000c Spectrophotometer. Sequencing libraries were  
1009 generated by Novogene Co., Ltd. using a NEBNext®Ultra™ RNA Library Prep Kit  
1010 for Illumina (NEB, USA) following the manufacturer's recommendations; index  
1011 codes were added to attribute sequences to each sample. The index-coded samples  
1012 were clustered using a HiSeq 4000 PE Cluster Kit (Illumina) according to the  
1013 manufacturer's instructions. After cluster generation, the libraries were sequenced on  
1014 an Illumina HiSeq 4000 platform as 150-bp paired-end reads. The clean reads were  
1015 aligned to the B73 reference genome (RefGen\_v5) through the HISAT2 program  
1016 (Kim et al., 2015). Differentially expressed genes (DEGs) were identified as meeting  
1017 the criteria of an absolute value of  $\log_2(\text{fold-change}) > 1$  and adjusted  $p$ -value  $< 0.05$   
1018 by the R package DESeq (Love et al., 2014).

### 1019 **DAP-seq**

1020 The *in vitro* DAP-seq was performed as described previously, with some minor  
1021 modifications (Allen et al., 2006; O'Malley et al., 2016; Bartlett et al., 2017).  
1022 Halo-tagged transcription factors (O2, ZmNAC128, and ZmNAC130) and  
1023 recombinant proteins were produced in a TNT Coupled Wheat Germ Extract System  
1024 (Promega). Genomic DNA was extracted from 8-, 12-, and 16-DAP maize kernels

1025 using a modified cetyltrimethylammonium bromide (CTAB) extraction method,  
1026 purified with a FastPure Gel DNA Extraction Mini Kit (Vazyme), and sonicated to  
1027 ~200-bp fragments. After end-repair and adenylation, the fragmented gDNA was then  
1028 purified using AMPure® XP Beads (Beckman Coulter). The Halo-tagged-TFs and  
1029 Halo proteins were bound to Magne HaloTag Beads (Promega) and subsequently  
1030 incubated with the fragmented gDNA library for 1 h on a rotator at room temperature.  
1031 The beads were then washed three times, and the eluted DNA was ligated to an  
1032 indexed adaptor for sequencing analysis. For peak analysis, the mapped reads and  
1033 peak files were examined using Integrative Genomics Viewer. Enriched motifs were  
1034 identified by MEME motif discovery software (<http://meme-suite.org/>). The primers  
1035 are listed in Supplemental Dataset S8.

#### 1036 **ChIP-qPCR**

1037 The 16-DAP developing endosperms of *ZmNAC128-3×Flag* and  
1038 *ZmNAC130-3×Flag* transgenic lines were fixed with 1% (v/v) formaldehyde (Sigma)  
1039 in phosphate buffer as described previously (Yang et al., 2021). Antibodies against  
1040 3×Flag peptide (F1804, Sigma) and Rabbit IgG control (Sigma, 12-370) were used for  
1041 immunoprecipitation. The experimental procedure is the same as described previously  
1042 (Yang et al., 2021; Li et al., 2015). The immunoprecipitated DNA was used for qPCR  
1043 experiments of target DNA fragments which were performed with SYBR Green  
1044 (Takara) on a CFX Connect Real-Time PCR system (Bio-Rad) according to the  
1045 standard operating manual. Relative enrichment of target DNA fragments was  
1046 calculated by analyzing the immunoprecipitated samples of anti-Flag compared to that  
1047 of anti-IgG. *ACTIN* is the internal reference gene in the detected samples with three  
1048 biological replicates. The primers are listed in Supplemental Dataset S8.

#### 1049 **EMSA**

1050 Oligonucleotide probes of the *O2* promoter were synthesized and labeled with  
1051 biotin at the 3' end with a Biotin 3' End DNA Labeling Kit (Thermo) according to the  
1052 standard procedures. Each probe was mixed with purified recombinant protein at  
1053 25°C for 20 min in reaction buffer (20 µL) containing 10× binding buffer, 50% (v/v)

1054 glycerol, 100 mM MgCl<sub>2</sub>, 1 µg/µL poly(dI-dC), 50 mM KCl, and 1% (v/v) NP-40.  
 1055 Biotin-labeled DNA was detected according to the instructions of the LightShift  
 1056 Chemiluminescent EMSA Kit (Thermo). The luminescence was visualized on a  
 1057 Tanon-5200M imaging system.

#### 1058 **DLR assay**

1059 Maize protoplasts were prepared from the leaves of two-weeks seedlings of the  
 1060 inbred B73. The protoplast isolation, polyethylene glycol (PEG)-calcium transfection  
 1061 of plasmid DNA, and protoplast culture were described previously (Zhang et al.,  
 1062 2015). The vector pRI101 (Clontech) was used for the expression of *O2*, *ZmNAC128*,  
 1063 and *ZmNAC130* under the control of the 35S promoter. The transient expression  
 1064 vector pGreenII 0800-LUC was used to generate the reporter constructs by cloning  
 1065 the promoters of different target genes upstream of LUC. The LUC/REN activity ratio  
 1066 was measured using a Dual-luciferase Reporter Assay System (Promega). The primers  
 1067 are listed in Supplemental Dataset S8.

#### 1068 **Statistical analysis**

1069 Data processing of means, standard deviations, and *p*-values was performed with  
 1070 Microsoft Excel (2016): AVERAGE, STDEV.S, and Student's *t*-test, respectively. The  
 1071 one-way ANOVA test in the SPSS software was employed to determine whether there  
 1072 are significant differences among three or more groups. Immunoblotting signals in  
 1073 each band were quantified by ImageJ (<https://imagej.nih.gov/ij/>). The *p*-value and  
 1074 false discovery rate (FDR) of differentially expressed genes in the RNA-seq data were  
 1075 calculated by the DESeq2R package (v 1.28.1 with default arguments). The raw data  
 1076 and detailed statistical analysis are in Supplemental Dataset S9.

#### 1077 **Accession numbers**

1078 *ZmNAC128*: Zm00001eb126890; *ZmNAC130*: Zm00001eb334180; *O2*:  
 1079 Zm00001eb301570; *16-kD γ-zein*: Zm00001eb099950; *27-kD γ-zein*:  
 1080 Zm00001eb313800; *50-kD γ-zein*: Zm00001eb313790; *Sus1*: Zm00001eb392880;  
 1081 *SSV*: Zm00001eb191890, *Bt2*: Zm00001eb176800; *SSIIa*: Zm00001eb279740; *GBSSI*:  
 1082 Zm00001eb378140; *SSI*: Zm00001eb376100; *Zpu1*: Zm00001eb088740; *SSIII*:

1083 Zm00001eb413290; *Sh2*: Zm00001eb159060; *SBEIIb*: Zm00001eb242610; *PPDK1*:  
1084 Zm00001eb287770; *PPDK2*: Zm00001eb349810; *Sh1*: Zm00001eb374090; *ISA1*:  
1085 Zm00001eb174590; *Bt1*: Zm00001eb235570; *ZmSWEET4c*: Zm00001eb236810;  
1086 *ZmSUGCARI*: Zm00001eb304390; *ZmYSL2*: Zm00001eb248990; *ZmMNI*:  
1087 Zm00001eb083790; *ACTIN*: Zm00001eb348450. The RNA-seq and DAP-seq data in  
1088 this article are available from the National Center for Biotechnology Information  
1089 Gene Expression Omnibus (<http://www.ncbi.nlm.nih.gov/geo>) under the series entries  
1090 PRJNA913969 for RNA-seq data and PRJNA914049 for DAP-seq data.

1091  
1092  
1093  
1094  
1095  
1096  
1097  
1098  
1099  
1100  
1101  
1102  
1103  
1104  
1105  
1106  
1107  
1108  
1109  
1110  
1111

1141

1142

1143

1144

1145

1146

1147

1148

1149

1150

1151

1152

1153

1154

1155

1156

1157

1158

1159

**1160 Funding information**

1161 This work was supported by the National Natural Science Foundation of China  
1162 (31671703 and 32072010 to Z.Z.), start-up funding from the University of Science  
1163 and Technology of China (KY9100000020 and WK9100000017 to Z.Z.), and the  
1164 Chinese Academy of Sciences (KJ2070000078 to Z.Z.).

1165

**1166 Acknowledgments**

1167 Dr. Joachim Messing's legacy lives on through this project, which owes its inception  
1168 to his visionary leadership and guidance. We also thank Dr. Xiaoduo Lu from the Qilu  
1169 Normal University for providing B73o2 mutants in an EMS-mutagenized maize

1170 inbred B73 library, Dr. Jihua Tang and Qiyue Wang from the Henan Agricultural  
 1171 University for the assistance of DAP-seq experiment, and Dr. Chunguang Chen and  
 1172 Yanwen Xiang from the Orizymes Biotechnologies (Shanghai) Co., Ltd. for the  
 1173 assistance of DAP-seq analyses and CHIP experiments.

1174

#### 1175 **Author contributions**

1176 Z.Z. supervised the project. Z.Z., E.C., J.H., and D.P. designed the experiments and  
 1177 wrote the manuscript. E.C., H.Y., J.H., and D.P. performed the experiments. P.Z., S.P.,  
 1178 X.W., J.W., and C.J. assisted with the field work, material sampling, and identification.  
 1179 Z.C. and D.C. measured and analyzed the element levels in the kernels. Z.X. and Y.W.  
 1180 analyzed seed composition. Y.W. helped conduct the project.

1181

#### 1182 **Tables**

1183 **Table 1.** Summary of promoter analysis of starch metabolism genes and their  
 1184 expression in *nacRNAi* and *zmnac128 zmnac130*.

Gene name	Binding peaks	Cis-element ACGCAA	<i>nacRNAi</i>		<i>zmnac128 zmnac130</i>	
			mRNA	Protein	mRNA	Protein
Bt2	Y	Y	down.	reduced	down.	reduced
Zpu1	Y	Y	down.	n.d.	down.	reduced
GBSS1	Y	Y	down.	n.d.	down.	reduced
SS1	Y	Y	down.	n.d.	down.	reduced
Sus1	Y	Y	down.	n.d.	down.	n.d.
SBEIIb	Y	N	down.	n.d.	down.	reduced
SSIIa	Y	Y	n.s.	n.d.	down.	reduced
ISA1	N	N	n.s.	n.d.	down.	reduced
Sh2	N	Y	n.s.	n.d.	n.s.	reduced
Sh1	N	Y	n.s.	n.d.	n.s.	reduced
SSIII	N	Y	n.s.	n.d.	n.s.	reduced
SSV	N	Y	n.s.	n.d.	n.s.	reduced
Bt1	Y	N	n.d.	n.d.	n.s.	reduced
SBE1	N	N	down.	n.d.	n.s.	n.s.

1185 Note: The data of *nacRNAi* from Zhang et al., 2019. The data of *zmnac128 zmnac130*  
 1186 from this study. Y, Yes (binding peaks detected in the promoter); N, No (ACGCAA



1187 element absent in the promoter); down., downregulated; n.d., no detection; n.s., not  
1188 significantly downregulated or reduced.

1189

## 1190 **Figure legends**

### 1191 **Figure 1. Knockout mutation of *ZmNAC128* and *ZmNAC130* causes poorly filled** 1192 **kernel phenotypes.**

1193 **(A)** Kernel phenotype of KN5585 (wild type, WT), *zmnac128*, *zmnac130*, and  
1194 *zmnac128 zmnac130*. Top, mature kernel longitudinal sections; middle and bottom,  
1195 scanning electron microscope of kernel longitudinal sections shown above. Middle,  
1196 kernel peripheral region; bottom, kernel inner region.

1197 **(B)** The hundred kernel weight (HKW) of mature kernels of the three mutants  
1198 compared to the WT. g, gram.

1199 **(C)** NIR analysis conducted to determine the percentage of protein and starch  
1200 accounting for kernel weight. The calibration of the NIR model utilized mature kernel  
1201 flours from various maize varieties, as explained in detail in the 'Materials and  
1202 Methods' section. The protein or starch content in each kernel is expressed as a  
1203 percentage (%) of kernel weight, calculated by comparing NIR-derived value to  
1204 kernel weight. Data represent means  $\pm$  standard deviation (SD) of at least three  
1205 independent samples for each genotype (**B** and **C**). Different lowercase letters indicate  
1206 significant differences according to a one-way ANOVA with Tukey's multiple  
1207 comparisons test ( $p < 0.05$ ).

### 1208 **Figure 2. RNA-seq combined with DAP-seq investigating the direct targets of** 1209 ***ZmNAC128* and *ZmNAC130*.**

1210 **(A)** Number of upregulated and downregulated expressed genes in *zmnac128*,  
1211 *zmnac130*, and *zmnac128 zmnac130*, compared to the WT. DEGs were identified  
1212 based on fold-change  $\geq 2$  and  $p$ -value  $\leq 0.05$ .

1213 **(B)** Significantly enriched GO terms and KEGG pathways based on DEGs of  
1214 *zmnac128 zmnac130*. GO:0046982 (protein heterodimerization activity); GO:0045735  
1215 (nutrient reservoir activity); ko00010 (glycolysis/gluconeogenesis); ko00500 (starch

1216 and sucrose metabolism); ko01200 (carbon metabolism); ko00620 (pyruvate  
1217 metabolism); ko00710 (carbon fixation in photosynthetic organisms); ko00520  
1218 (amino sugar and nucleotide sugar metabolism); ko00630 (glyoxylate and  
1219 dicarboxylate metabolism); ko00030 (pentose phosphate pathway); ko00052  
1220 (galactose metabolism); ko01230 (biosynthesis of amino acids); ko00260 (glycine,  
1221 serine and threonine metabolism); ko01212 (fatty acid metabolism).

1222 **(C)** Distribution of ZmNAC128 and ZmNAC130 binding regions in the maize  
1223 genome. **(D)** Metaplots showing the distribution of ZmNAC128 and ZmNAC130  
1224 binding peaks per 100-bp bin corresponding to the -1,000- to +2,000-bp region  
1225 flanking the transcription start site (TSS).

1226 **(E)** IGV shows the distribution of ZmNAC128- and ZmNAC130-binding peaks in the  
1227 promoters of *16-kD  $\gamma$ -zein* and *Bt2*. For ZmNAC128, ZmNAC130, and IgG (control),  
1228 two independent experiments were performed. Aligned reads are indicated in red  
1229 (ZmNAC128), orange (ZmNAC130), or gray (IgG). The y-axis (or peaks) represents  
1230 the number (or accumulation) of the aligned reads. The relative positions of the  
1231 element ACGCAA are marked by arrowheads.

1232 **(F)** The most significant elements of ZmNAC128 and ZmNAC130 according to  
1233 MEME-ChIP analysis.

1234 **Figure 3. Verification of 27-kD  $\gamma$ -zein and 50-kD  $\gamma$ -zein as the direct targets of**  
1235 **ZmNAC128 and ZmNAC130.**

1236 **(A)** IGV shows the peaks bound by ZmNAC128 and ZmNAC130 in these two  
1237 promoters. The relative positions of the element ACGCAA are marked by arrowheads.

1238 **(B)** ChIP-qPCR detects the *in vivo* binding activities of ZmNAC128 and ZmNAC130  
1239 to these two promoters. The red lines under the arrowheads in **(A)** indicate the region  
1240 detected by ChIP-qPCR. ChIP products of IgG were used as a negative control.  
1241 *ACTIN* was used as an internal control.

1242 **(C)** DLR detects the transactivation activities of ZmNAC128 and ZmNAC130 on the  
1243 two promoters. The results were also shown in **Supplemental Figure S17**. Data  
1244 represent means  $\pm$  SD of three independent samples for each test **(B and C)**.

1245 Significance differences ( $***p < 0.001$ ) were determined by a Student's *t*-test (**B**).  
1246 Different lowercase letters indicate significant differences according to a one-way  
1247 ANOVA with Tukey's multiple comparisons test ( $p < 0.05$ ) (**C**).

1248 **Figure 4. Verification of starch metabolism genes as direct targets of ZmNAC128**  
1249 **and ZmNAC130.**

1250 **(A)** Immunoblotting of protein accumulation for the major starch metabolism  
1251 enzymes in 20-DAP endosperms of *zmnac128 zmnac130* and WT. The 20 ng non-zein  
1252 proteins per lane were loaded, while ACTIN served as the loading control. The  
1253 original and intact images were shown in **Supplemental Figure S21**. Three  
1254 independent samples for each material were performed and quantified by the ImageJ  
1255 software. For each starch metabolism enzyme, protein abundance in *zmnac128*  
1256 *zmnac130* was normalized to the corresponding WT, which was set to 1.

1257 **(B)** IGV shows binding peaks in the promoters of genes transcriptionally  
1258 downregulated in *zmnac128 zmnac130*. The relative positions of the cis-element  
1259 ACGCAA are marked by arrowheads.

1260 **(C)** ChIP-qPCR detects the *in vivo* binding activities of ZmNAC128 and ZmNAC130  
1261 to the five promoters. The red lines under the arrowheads in **(B)** indicate the region  
1262 detected by ChIP-qPCR.

1263 **(D)** DLR detects the transactivation activities of ZmNAC128 and ZmNAC130 on  
1264 these five promoters. Data represent means  $\pm$  SD of three independent samples for  
1265 each test (**A**, **C**, and **D**). Significance differences ( $**p < 0.01$  and  $***p < 0.001$ ) were  
1266 determined by a Student's *t*-test (**A** and **C**). Different lowercase letters indicate  
1267 significant differences according to a one-way ANOVA with Tukey's multiple  
1268 comparisons test ( $p < 0.05$ ) (**D**).**Figure 5. ZmNAC128 and ZmNAC130 regulate**  
1269 **the expression of O2 in the filling endosperm.**

1270 **(A)** RT-qPCR of *O2* expression in the filling endosperms of *zmnac128 zmnac130* and  
1271 WT. Relative expression was normalized to *ACTIN*. Data represent means  $\pm$  SD of  
1272 three independent samples for each time point except for two samples at 28 DAP.  
1273 Statistical significance was determined by a Student's *t*-test.  $*p < 0.05$ ,  $**p < 0.01$ ,

1274 \*\*\* $p < 0.001$ .

1275 **(B)** Immunoblotting of O2 protein in the filling endosperms of *zmnac128 zmnac130*  
1276 and WT. The 20 ng non-zein proteins per lane were loaded. The quantification was  
1277 shown in **Supplemental Figure S8**.

1278 **(C)** IGV shows the peaks bound by ZmNAC128 and ZmNAC130 in the O2 promoter.  
1279 The relative region covering four candidate elements, CATGCATG, GTACGT,  
1280 CTAGCTA, and TTGCTT, are marked by a red line in the promoter.

1281 **(D)** EMSA detects an additional cis-element of ZmNAC128 and ZmNAC130 in the  
1282 O2 promoter. Upside: five biotin-labeled probes in the region of -510 to -360  
1283 upstream from the start codon are listed, and candidate cis-elements in the probe  
1284 sequences are highlighted in red font. Underside: the 6-bp GTACGT box in the P3  
1285 probe (WT) and three mutant probes were produced by 2-bp mutations in the 6-bp  
1286 box.

1287 **(E)** ChIP-qPCR detects the *in vivo* binding activity of ZmNAC128 and ZmNAC130  
1288 to the O2 promoter. A red line in the O2 promoter in (C) indicates the region detected  
1289 by ChIP-qPCR.

1290 **(F)** DLR detects the transactivation activities of ZmNAC128 and ZmNAC130 on the  
1291 O2 promoter. Data represent means  $\pm$  SD of three independent samples for each test  
1292 **(E and F)**. Significance differences (\*\* $p < 0.01$  and \*\*\* $p < 0.001$ ) were determined  
1293 by a Student's *t*-test **(E)**. Different lowercase letters indicate significant differences  
1294 according to a one-way ANOVA with Tukey's multiple comparisons test ( $p < 0.05$ )  
1295 **(F)**.

1296 **Figure 6. *In vitro* and *in vivo* protein interaction assays show the physical**  
1297 **interaction of O2, ZmNAC128, and ZmNAC130.**

1298 **(A)** GST pull-down detects the interactions between recombinant purified proteins of  
1299 O2, ZmNAC128, and ZmNAC130.

1300 **(B)** BiFC detects the interactions between O2, ZmNAC128, and ZmNAC130.  
1301 Negative controls in **Supplemental Figure S11**. BF, bright field. Scale bars, 50  $\mu$ m.

1302 **(C)** Co-IP detects the interactions between O2, ZmNAC128, and ZmNAC130. The

1303 indicated plasmids (harboring Flag or Myc tags) were transformed and subsequently  
1304 co-expressed in *N. benthamiana* leaves. The Flag-fused proteins were  
1305 immunoprecipitated, and the precipitates were probed with anti-Flag or anti-Myc  
1306 antibodies.

1307 **Figure 7. The triple mutation of *O2*, *ZmNAC128*, and *ZmNAC130* causes a more**  
1308 **poorly filled kernel phenotype.**

1309 (A) Mature cobs and kernel longitudinal sections of *o2*, *zmnac128 zmnac130*, and  
1310 *zmnac128 zmnac130 o2* compared to the NT in the KN5585 × B73 background.

1311 (B) The hundred-kernel weight (HKW) analysis of the four genetic materials.

1312 (C) Determination of protein and starch in the mature kernels from the four genetic  
1313 materials. Data represent means ± SD of at least three independent samples for each  
1314 genotype (B and C). Different lowercase letters indicate significant differences  
1315 according to a one-way ANOVA with Tukey's multiple comparisons test ( $p < 0.05$ ) (B  
1316 and C).

1317 **Figure 8. *O2*, *ZmNAC128*, and *ZmNAC130* synergistically affect the expression**  
1318 **of zeins and starch metabolism enzymes.**

1319 (A) Principal component analysis based on transcriptome data of the four genetic  
1320 materials. There were three independent samples for each genotype.

1321 (B) Number of DEGs in *o2*, *zmnac128 zmnac130*, and *zmnac128 zmnac130 o2*  
1322 compared to the NT. DEGs were identified based on fold-change  $\geq 2$  and  $p$ -value  $\leq$   
1323 0.05.

1324 (C) Venn diagram shows the overlap between these DEGs.

1325 (D) Coomassie Brilliant Blue staining SDS-PAGE of zein proteins in mature kernels.  
1326 The total zein proteins loaded in each lane are equal to 200  $\mu\text{g}$  of mature kernel flour.  
1327 Each band was indicated by the corresponding type of zein. 50 $\gamma$ , 50-kD  $\gamma$ -zein; 27 $\gamma$ ,  
1328 27-kD  $\gamma$ -zein; 22 $\alpha$ , 22-kD  $\alpha$ -zein; 19 $\alpha$ , 19-kD  $\alpha$ -zein; 16 $\gamma$ , 16- kD  $\gamma$ -zein; 15 $\beta$ , 15-kD  
1329  $\beta$ -zein; 10 $\delta$ , 10-kD  $\delta$ -zein.

1330 (E) Immunoblotting of protein accumulation of starch metabolism enzymes in the  
1331 20-DAP endosperm. The 20 ng non-zein proteins for each lane were loaded, while

1332 ACTIN was the loading control.

1333 **Figure 9. ZmNAC128 and ZmNAC130 regulate the expression of ZmSWEET4c,**  
1334 **ZmSUGCAR1, and ZmYSL2.**

1335 (A) RNA *in situ* hybridization of *ZmNAC128* and *ZmNAC130* in 12-DAP B73 kernels.  
1336 Antisense probes were used to detect the spatial expression of *ZmNAC128* and  
1337 *ZmNAC130* transcripts. Sense probes were the negative controls. SE, starchy  
1338 endosperm; AL, aleurone; BETL, basal endosperm transfer layer. Scale bars, 100  $\mu\text{m}$ .

1339 (B) Expression levels of *ZmSWEET4c*, *ZmSUGCAR1*, *ZmYSL2*, and *ZmMNI* in the  
1340 16-DAP endosperms of *zmnac128 zmnac130* versus WT in the KN5585 background.  
1341 Expression levels are shown as FPKM (fragments per kilobase of exon per million  
1342 mapped reads). Statistical significance was determined by DESeq2R. \*\* $p < 0.01$ ;  
1343 \*\*\* $p < 0.001$ .

1344 (C) IGV shows the peaks bound by ZmNAC128 and ZmNAC130 in the four  
1345 promoters. The relative positions of the element GTACGT are marked by arrowheads.

1346 (D) ChIP-qPCR detects the *in vivo* binding activities of ZmNAC128 and ZmNAC130  
1347 to the promoters of *ZmSWEET4c*, *ZmSUGCAR1*, and *ZmYSL2*. The red lines under the  
1348 arrowheads in (C) indicate the region detected by ChIP-qPCR. Data represent means  
1349  $\pm$  SD of three independent samples for each test. Statistical significance was  
1350 determined by a Student's *t*-test. \*\* $p < 0.01$ ; ns, not significant.

1351 (E) DLR detects the transactivation activities of ZmNAC128, ZmNAC130, and O2 on  
1352 the four promoters. The data was also shown in **Supplemental Figure S19B**  
1353 combined with the transactivation of O2, ZmNAC128, and ZmNAC130 on the four  
1354 promoters. Data represent means  $\pm$  SD of three independent samples for each test.  
1355 Different lowercase letters indicate significant differences according to a one-way  
1356 ANOVA with Tukey's multiple comparisons test ( $p < 0.05$ ).

1357 **Figure 10. Mutations in O2, ZmNAC128, and ZmNAC130 influence soluble sugar**  
1358 **and element levels in kernels, and a working model of these three TFs facilitates**  
1359 **endosperm filling.**

1360 (A) Determination of soluble sugars (glucose, fructose, and sucrose) and elements (Zn,

1361 Fe, and K) in the mature kernels of NT, *o2*, *zmnac128 zmnac130*, and *zmnac128*  
1362 *zmnac130 o2* in the KN5585 × B73 background. Data represent means ± SD of three  
1363 independent samples in sugar measurement and six independent samples in element  
1364 measurement for each genotype. Different lowercase letters indicate significant  
1365 differences according to a one-way ANOVA with Tukey's multiple comparisons test ( $p$   
1366 < 0.05).

1367 **(B)** A working model of O2, ZmNAC128, and ZmNAC130 facilitates endosperm  
1368 filling. Left panel, a cartoon illustration depicts the cooperation of the three TFs to  
1369 promote endosperm filling. Maternal nutrients are transported via the BETL into the  
1370 starchy endosperm for synthesis and deposition of storage reserves (starch and zeins).  
1371 Right panel, the major targets of ZmNAC128 and ZmNAC130 have been  
1372 characterized in this study except for *16-kD γ-zein* and *Bt2* which have been  
1373 previously investigated (Zhang et al., 2019). Arrows indicate direct transcriptional  
1374 regulation.

1375

## 1376 **References**

- 1377 **Allen GC, Flores-Vergara MA, Krasynanski S, Kumar S, and Thompson WF (2006).** A  
1378 modified protocol for rapid DNA isolation from plant tissues using  
1379 cetyltrimethylammonium bromide. *Nat Protoc* **1**, 2320-2325.
- 1380 **Bartlett A, O'Malley RC, Huang SC, Galli M, Nery JR, Gallavotti A, and Ecker JR (2017).**  
1381 Mapping genome-wide transcription-factor binding sites using DAP-seq. *Nat Protoc* **12**,  
1382 1659-1672.
- 1383 **Becraft PW and Asuncion-Crabb Y (2000).** Positional cues specify and maintain aleurone cell  
1384 fate in maize endosperm development. *Development* **127**, 4039-4048.
- 1385 **Becraft PW and Gutierrez-Marcos J (2012).** Endosperm development: dynamic processes and  
1386 cellular innovations underlying sibling altruism. *Wiley Interdiscip Rev Dev Biol* **1**,

1387 579-593.

1388 **Becraft PW, Stinard PS, and McCarty DR** (1996). CRINKLY4: A TNFR-like receptor kinase  
1389 involved in maize epidermal differentiation. *Science* **273**, 1406-1409.

1390 **Boston RS and Larkins BA** (2009). The Genetics and Biochemistry of Maize Zein Storage  
1391 Proteins. In *Handbook of Maize: Genetics and Genomics*, J.L. Bennetzen and S. Hake,  
1392 eds (New York, NY: Springer New York), pp. 715-730.

1393 **Chao Z, Chen Y, Ji C, Wang Y, Huang X, Zhang C, Yang J, Song T, Wu J, Guo L, Liu C, Han**  
1394 **M, Wu Y, Yan J, and Chao D** (2022). A genome-wide association study identifies a  
1395 transporter for zinc uploading to maize kernels. *EMBO Rep*, e55542.

1396 **Chen J, Zeng B, Zhang M, Xie S, Wang G, Hauck A, and Lai J** (2014). Dynamic Transcriptome  
1397 Landscape of Maize Embryo and Endosperm Development. *Plant Physiol* **166**,  
1398 252-264.

1399 **Cheng WH, Taliercio EW, and Chourey PS** (1996). The Miniature1 Seed Locus of Maize  
1400 Encodes a Cell Wall Invertase Required for Normal Development of Endosperm and  
1401 Maternal Cells in the Pedicel. *Plant Cell* **8**, 971-983.

1402 **Chourey PS and Hueros G** (2017). The Basal Endosperm Transfer Layer(BETL): Gateway to  
1403 the Maize Kernel. In *Maize Kernel Development*, B.A. Larkins, ed (Boston, MA: CABI),  
1404 pp. 56-67.

1405 **Costa LM, Yuan J, Rouster J, Paul W, Dickinson H, and Gutierrez-Marcos JF** (2012). Maternal  
1406 control of nutrient allocation in plant seeds by genomic imprinting. *Curr Biol* **22**,  
1407 160-165.

1408 **Dai D, Ma Z, and Song R** (2021). Maize Endosperm Development. *J Integr Plant Biol* **63**,



1409 613-627

1410 **Deng Y, Wang J, Zhang Z, and Wu Y** (2020). Transactivation of *Sus1* and *Sus2* by *Opaque2* is  
1411 an essential supplement to sucrose synthase-mediated endosperm filling in maize.  
1412 *Plant Biotechnol J* **18**, 1897-1907.

1413 **Feng F, Qi W, Lv Y, Yan S, Xu L, Yang A, Yuan Y, Chen Y, Zhao H, and Song R** (2018).  
1414 *OPAQUE11* Is a Central Hub of the Regulatory Network for Maize Endosperm  
1415 Development and Nutrient Metabolism. *Plant Cell* **30**, 375-396.

1416 **Flint-Garcia SA** (2017). Kernel evolution: From teosinte to maize. In *Maize Kernel*  
1417 Development, B.A. Larkins, ed (Boston, MA: CABI), pp. 1-16.

1418 **Flint-Garcia SA, Bodnar AL, and Scott MP** (2009). Wide variability in kernel composition, seed  
1419 characteristics, and zein profiles among diverse maize inbreds, landraces, and  
1420 teosinte. *Theoretical and Applied Genetics* **119**, 1129-1142.

1421 **Frame B, Main M, Schick R, and Wang K** (2011). Genetic transformation using maize  
1422 immature zygotic embryos. *Methods Mol Biol* **710**, 327-341.

1423 **Galli M, Khakhar A, Lu Z, Chen Z, Sen S, Joshi T, Nemhauser J, Schmitz R, and Gallavotti A**  
1424 (2018). The DNA binding landscape of the maize AUXIN RESPONSE FACTOR family.  
1425 *Nature Communications* **9**, 4526.

1426 **Gao Y, An K, Guo W, Chen Y, Zhang R, Zhang X, Chang S, Rossi V, Jin F, Cao X, Xin M,**  
1427 **Peng H, Hu Z, Guo W, Du J, Ni Z, Sun Q, and Yao Y** (2021). The endosperm-specific  
1428 transcription factor *TaNAC019* regulates glutenin and starch accumulation and its elite  
1429 allele improves wheat grain quality. *Plant Cell* **33**, 603-622.

1430 **Gomez E, Royo J, Guo Y, Thompson R, and Hueros G** (2002). Establishment of cereal

1431 endosperm expression domains: identification and properties of a maize transfer  
1432 cell-specific transcription factor, ZmMRP-1. *Plant Cell* **14**, 599-610.

1433 **Gomez E, Royo J, Muniz LM, Sellam O, Paul W, Gerentes D, Barrero C, Lopez M, Perez P,**  
1434 **and Hueros G** (2009). The Maize Transcription Factor Myb-Related Protein-1 Is a Key  
1435 Regulator of the Differentiation of Transfer Cells. *Plant Cell* **21**, 2022-2035.

1436 **Gontarek BC, Neelakandan AK, Wu H, and Becraft PW** (2016). NKD Transcription Factors Are  
1437 Central Regulators of Maize Endosperm Development. *Plant Cell* **28**, 2916-2936.

1438 **Guan H, Dong Y, Lu S, Liu T, He C, Liu C, Liu Q, Dong R, Wang J, Li Y, Qi S, and Wang L**  
1439 (2020). Characterization and map-based cloning of miniature2-m1, a gene controlling  
1440 kernel size in maize. *J Integr Agric* **19**, 1961–1973.

1441 **Hannah LC and Boehlein S** (2017). Starch biosynthesis in maize endosperm. In *Maize kernel*  
1442 *development*, B.A. Larkins, ed (Boston, MA: CABI), pp. 149–159.

1443 **He Y, Yang Q, Yang J, Wang Y, Sun X, Wang S, Qi W, Ma Z, and Song R** (2021). shrunken4  
1444 is a mutant allele of ZmYSL2 that affects aleurone development and starch synthesis  
1445 in maize. *Genetics* **218**, iyab070.

1446 **Huang J, Xu W, Zhai J, Hu Y, Guo J, Zhang C, Zhao Y, Zhang L, Martine C, Ma H, Huang C**  
1447 (2023). Nuclear phylogeny and insights into whole-genome duplications and  
1448 reproductive development of Solanaceae plants. *Plant Communications*, 100595

1449 **Huang L, Tan H, Zhang C, Li Q, and Liu Q** (2021). Starch biosynthesis in cereal endosperms:  
1450 An updated review over the last decade. *Plant Commun* **2**, 100237.

1451 **Jin P, Guo T, and Becraft PW** (2000). The maize CR4 receptor-like kinase mediates a growth  
1452 factor-like differentiation response. *Genesis* **27**, 104-116. **Kim D, Langmead B,**

1453 **Salzberg SL** (2015) HISAT: a fast spliced aligner with low memory requirements.  
1454 Nature Methods **12**, 357-360.

1455 **Larkins BA, Wu Y, Song R, and Messing J** (2017). Maize seed storage proteins. In Maize  
1456 kernel development, B.A. Larkins, ed (Boston, MA: CABI), pp. 157-189.

1457 **Lending CR and Larkins BA** (1989). Changes in the zein composition of protein bodies during  
1458 maize endosperm development. Plant Cell **1**, 1011-1023.

1459 **Leroux BM, Goodyke AJ, Schumacher KI, Abbott CP, Clore AM, Yadegari R, Larkins BA, and**  
1460 **Dannenhoffer JM** (2014). Maize early endosperm growth and development: from  
1461 fertilization through cell type differentiation. Am J Bot **101**, 1259-1274.

1462 **Li C and Song R** (2020). The regulation of zein biosynthesis in maize endosperm. Theor Appl  
1463 Genet **133**, 1443-1453.

1464 **Li C, Yue Y, Chen H, Qi W, and Song R** (2018). The ZmbZIP22 Transcription Factor Regulates  
1465 27-kD gamma-Zein Gene Transcription during Maize Endosperm Development. The  
1466 Plant Cell **30**, 2402-2424.

1467 **Li C, Qiao Z, Qi W, Wang Q, Yuan Y, Yang X, Tang Y, Mei B, Lv Y, Zhao H, Xiao H, and Song**  
1468 **R** (2015). Genome-Wide Characterization of cis-Acting DNA Targets Reveals the  
1469 Transcriptional Regulatory Framework of Opaque2 in Maize. The Plant Cell **27**,  
1470 532-545.

1471 **Li Q and Wu Y** (2020). The encyclopedia of maize kernel gene expression. J Integr Plant Biol  
1472 **62**, 879-881.

1473 **Lid SE, Gruis D, Jung R, Lorentzen JA, Ananiev E, Chamberlin M, Niu X, Meeley R, Nichols S,**  
1474 **and Olsen OA** (2002). The defective kernel 1 (dek1) gene required for aleurone cell

1475 development in the endosperm of maize grains encodes a membrane protein of the  
1476 calpain gene superfamily. *Proc Natl Acad Sci U S A* **99**, 5460-5465.

1477 **Liu Y, Hou J, Wang X, Li T, Majeed U, Hao C, and Zhang X** (2020). The NAC transcription  
1478 factor NAC019-A1 is a negative regulator of starch synthesis in wheat developing  
1479 endosperm. *J Exp Bot* **71**, 5794-5807.

1480 **Livak KJ and Schmittgen TD** (2001). Analysis of Relative Gene Expression Data Using  
1481 Real-Time Quantitative PCR and the  $2^{-\Delta\Delta CT}$  Method. *Methods* **25**, 402-408.

1482 **Lynch JM and Barbano DM** (1999). Kjeldahl Nitrogen Analysis as a Reference Method for  
1483 Protein Determination in Dairy Products. *Journal of AOAC INTERNATIONAL* **82**,  
1484 1389-1398.

1485 **Lohmer S, Maddaloni M, Motto M, Di Fonzo N, Hartings H, Salamini F, and Thompson RD**  
1486 (1991). The maize regulatory locus Opaque-2 encodes a DNA-binding protein which  
1487 activates the transcription of the b-32 gene. *Embo J* **10**, 617-624.

1488 **Love MI, Huber W, and Anders S** (2014). Moderated estimation of fold change and dispersion  
1489 for RNA-seq data with DESeq2. *Genome Biol* **15**, 550.

1490 **Ning L, Wang Y, Shi X, Zhou L, Ge M, Liang S, Wu Y, Zhang T, and Zhao H** (2022).  
1491 Nitrogen-dependent binding of the transcription factor PBF1 contributes to the balance  
1492 of protein and carbohydrate storage in maize endosperm. *Plant Cell* **35**, 409-434

1493 **O'Malley RC, Huang SC, Song L, Lewsey MG, Bartlett A, Nery JR, Galli M, Gallavotti A, and**  
1494 **Ecker JR** (2016). Cistrome and Epicistrome Features Shape the Regulatory DNA  
1495 Landscape. *Cell* **166**, 1598.

1496 **Olsen OA** (2001). ENDOSPERM DEVELOPMENT: Cellularization and Cell Fate Specification.

1497 Annu Rev Plant Physiol Plant Mol Biol **52**, 233-267.

1498 **Pysh LD, Aukerman MJ, and Schmidt RJ** (1993). OHP1: a maize basic domain/leucine zipper  
1499 protein that interacts with opaque2. The Plant Cell **5**, 227-236.

1500 **Qiao Z, Qi W, Wang Q, Feng Y, Yang Q, Zhang N, Wang S, Tang Y, and Song R** (2016).  
1501 ZmMADS47 Regulates Zein Gene Transcription through Interaction with Opaque2.  
1502 Plos Genetics **12**, 1005991.

1503 **Sabelli PA and Larkins BA** (2009). The development of endosperm in grasses. Plant Physiol  
1504 **149**, 14-26.

1505 **Schmidt RJ, Burr FA, and Burr B** (1987). Transposon tagging and molecular analysis of the  
1506 maize regulatory locus opaque-2. Science **238**, 960-963.

1507 **Schmidt RJ, Burr FA, Aukerman MJ, and Burr B** (1990). Maize Regulatory Gene Opaque-2  
1508 Encodes a Protein with a Leucine-Zipper Motif That Binds to Zein DNA. Proc Natl  
1509 Acad Sci USA **87**, 46-50.

1510 **Shen B, Li C, Min Z, Meeley RB, Tarczynski MC, and Olsen OA** (2003). sal1 determines the  
1511 number of aleurone cell layers in maize endosperm and encodes a class E vacuolar  
1512 sorting protein. Proc Natl Acad Sci U S A **100**, 6552-6557.

1513 **Sosso D, Luo D, Li Q, Sasse J, Yang J, Gendrot G, Suzuki M, Koch KE, McCarty DR, Chourey**  
1514 **PS, Rogowsky PM, Ross-Ibarra J, Yang B, and Frommer WB** (2015). Seed filling in  
1515 domesticated maize and rice depends on SWEET-mediated hexose transport. Nat  
1516 Genet **47**, 1489-1493.

1517 **VicenteCarbajosa J, Moose SP, Parsons RL, and Schmidt RJ** (1997). A maize zinc-finger  
1518 protein binds the prolamin box in zein gene promoters and interacts with the basic

1519 leucine zipper transcriptional activator Opaque2. Proc Natl Acad Sci USA **94**,  
1520 7685-7690.

1521 **Wang E, Wang J, Zhu X, Hao W, Wang L, Li Q, Zhang L, He W, Lu B, Lin H, Ma H, Zhang G,**  
1522 **and He Z** (2008). Control of rice grain-filling and yield by a gene with a potential  
1523 signature of domestication. Nat Genet **40**, 1370-1374.

1524 **Wang J, Chen Z, Zhang Q, Meng S, and Wei C** (2020). The NAC Transcription Factors  
1525 OsNAC20 and OsNAC26 Regulate Starch and Storage Protein Synthesis. Plant  
1526 Physiol **184**, 1775-1791.

1527 **Wei Y, Ren Z, Wang B, Zhang L, Zhao Y, Wu J, Li L, Zhang X, and Zhao X** (2021). A nitrate  
1528 transporter encoded by ZmNPF7.9 is essential for maize seed development. Plant Sci  
1529 **308**, 110901.

1530 **Widiez T, Ingram GC, and F., G.-M.J.** (2017). Embryo–Endosperm–Sporophyte Interactions in  
1531 Maize Seeds. In Maize Kernel Development, B.A. Larkins, ed (Boston, MA: CABI), pp.  
1532 108-118.

1533 **Wu Y and Messing J** (2012). Rapid Divergence of Prolamin Gene Promoters of Maize After  
1534 Gene Amplification and Dispersal. Genetics **192**, 507-519.

1535 **Wu Y, Holding DR, and Messing J** (2010). gamma-Zeins are essential for endosperm  
1536 modification in quality protein maize. Proc Natl Acad Sci USA **107**, 12810-12815.

1537 **Xin M, Yang R, Li G, Chen H, Laurie J, Ma C, Wang D, Yao Y, Larkins BA, Sun Q, Yadegari R,**  
1538 **Wang X, and Ni Z** (2013). Dynamic expression of imprinted genes associates with  
1539 maternally controlled nutrient allocation during maize endosperm development. Plant  
1540 Cell **25**, 3212-3227.

1541 **Xu J and Messing J** (2008). Organization of the prolamin gene family provides insight into the  
1542 evolution of the maize genome and gene duplications in grass species. *Proc Natl Acad*  
1543 *Sci USA* **105**, 14330-14335.

1544 **Yang B, Wang J, Yu M, Zhang M, Zhong Y, Wang T, Liu P, Song W, Zhao H, Fastner A, Suter**  
1545 **M, Rentsch D, Ludewig U, Jin W, Geiger D, Hedrich R, Braun DM, Koch KE, McCarty**  
1546 **DR, Wu W, Li X, Wang Y, and Lai J** (2022). The sugar transporter ZmSUGCAR1 of  
1547 the Nitrate Transporter 1/Peptide Transporter family is critical for maize grain filling.  
1548 *Plant Cell* **34**, 4232-4254.

1549 **Yang T, Wu X, Wang W, and Wu Y** (2023). Regulation of seed storage protein synthesis in  
1550 monocot and dicot plants: A comparative review. *Mol Plant* **16**, 145-167.

1551 **Yang T, Guo L, Ji C, Wang H, Wang J, Zheng X, Xiao Q, and Wu Y** (2021). The B3  
1552 domain-containing transcription factor ZmABI19 coordinates expression of key factors  
1553 required for maize seed development and grain filling. *Plant Cell* **33**, 104-128.

1554 **Yang T, Wang H, Guo L, Wu X, Xiao Q, Wang J, Wang Q, Ma G, Wang W, and Wu Y** (2022).  
1555 ABA-induced Phosphorylation of basic Leucine Zipper 29, ABSCISIC ACID  
1556 INSENSITIVE 19 and Opaque2 by SnRK2.2 Enhances Gene Transactivation for  
1557 Endosperm Filling in Maize. *Plant Cell* **34**, 1933-1956.

1558 **Yi F, Gu W, Chen J, Song N, Gao X, Zhang X, Zhou Y, Ma X, Song W, Zhao H, Esteban E,**  
1559 **Pasha A, Provart NJ, and Lai J** (2019). High Temporal-Resolution Transcriptome  
1560 Landscape of Early Maize Seed Development. *Plant Cell* **31**, 974-992.

1561 **Yi G, Lauter AM, Scott MP, and Becraft PW** (2011). The thick aleurone1 mutant defines a  
1562 negative regulation of maize aleurone cell fate that functions downstream of defective

1563 kernel1. *Plant Physiol* **156**, 1826-1836.

1564 **Yi G, Neelakandan AK, Gontarek BC, Vollbrecht E, and Becraft PW** (2015). The naked  
1565 endosperm genes encode duplicate INDETERMINATE domain transcription factors  
1566 required for maize endosperm cell patterning and differentiation. *Plant Physiol* **167**,  
1567 443-456.

1568 **Zhan J, Dannenhoffer JM, and Yadegari R** (2017). Endosperm Development and  
1569 CellSpecialization. In *Maize Kernel Development*, B.A. Larkins, ed (Boston, MA: CABI),  
1570 pp. 28-43.

1571 **Zhan J, Li G, Ryu CH, Ma C, Zhang S, Lloyd A, Hunter BG, Larkins BA, Drews GN, Wang X,**  
1572 **and Yadegari R** (2018). Opaque-2 Regulates a Complex Gene Network Associated  
1573 with Cell Differentiation and Storage Functions of Maize Endosperm. *The Plant Cell* **30**,  
1574 2425-2446.

1575 **Zhan J, Thakare D, Ma C, Lloyd A, Nixon NM, Arakaki AM, Burnett WJ, Logan KO, Wang D,**  
1576 **Wang X, Drews G, and Yadegaria R** (2015). RNA Sequencing of Laser-Capture  
1577 Microdissected Compartments of the Maize Kernel Identifies Regulatory Modules  
1578 Associated with Endosperm Cell Differentiation. *Plant Cell* **27**, 513-531.

1579 **Zhang Y, Liu T, Meyer CA, Eeckhoutte J, Johnson DS, Bernstein BE, Nusbaum C, Myers RM,**  
1580 **Brown M, Li W, Liu XS** (2008). Model-based analysis of ChIP-Seq (MACS). *Genome*  
1581 *Biology* **9**, R137.**Zhang Z, Yang J, and Wu Y** (2015). Transcriptional Regulation of  
1582 Zein Gene Expression in Maize through the Additive and Synergistic Action of  
1583 opaque2, Prolamine-Box Binding Factor, and O2 Heterodimerizing Proteins. *The Plant*  
1584 *Cell* **27**, 1162-1172.



1585 **Zhang Z, Zheng X, Yang J, Messing J, and Wu Y** (2016). Maize endosperm-specific  
1586 transcription factors O2 and PBF network the regulation of protein and starch  
1587 synthesis. *Proc Natl Acad Sci U S A* **113**, 10842-10847.

1588 **Zhang Z, Dong J, Ji C, Wu Y, and Messing J** (2019). NAC-type transcription factors regulate  
1589 accumulation of starch and protein in maize seeds. *Proc Natl Acad Sci USA* **116**,  
1590 11223-11228.

1591 **Zhou L, Liu C, Chen Q, Wang W, Yao S, Zhao Z, Zhu S, Hong X, Xiong Y, and Cai Y** (2021).  
1592 Fine mapping and candidate gene analysis of maize defective kernel mutant dek54.  
1593 *Acta Agron Sin* **47**, 1903–1912.  
1594

ACCEPTED MANUSCRIPT

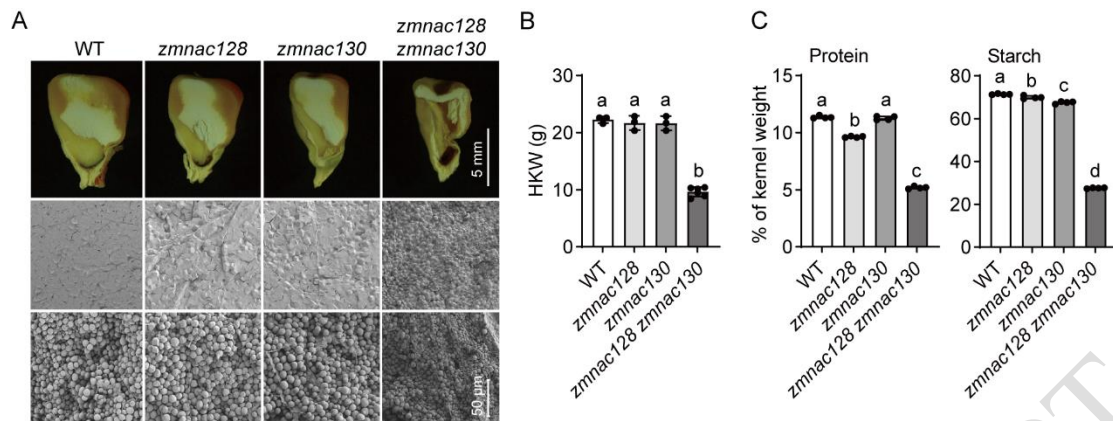


**Figure 1. Knockout mutation of *ZmNAC128* and *ZmNAC130* causes poorly filled kernel phenotypes.**

**(A)** Kernel phenotype of KN5585 (wild type, WT), *zmnac128*, *zmnac130*, and *zmnac128 zmnac130*. Top, mature kernel longitudinal sections; middle and bottom, scanning electron microscope of kernel longitudinal sections shown above. Middle, kernel peripheral region; bottom, kernel inner region.

**(B)** The hundred kernel weight (HKW) of mature kernels of the three mutants compared to the WT. g, gram.

**(C)** NIR analysis conducted to determine the percentage of protein and starch accounting for kernel weight. The calibration of the NIR model utilized mature kernel flours from various maize varieties, as explained in detail in the 'Materials and Methods' section. The protein or starch content in each kernel is expressed as a percentage (%) of kernel weight, calculated by comparing NIR-derived value to kernel weight. Data represent means  $\pm$  standard deviation (SD) of at least three independent samples for each genotype (**B** and **C**). Different lowercase letters indicate significant differences according to a one-way ANOVA with Tukey's multiple comparisons test ( $p < 0.05$ ).

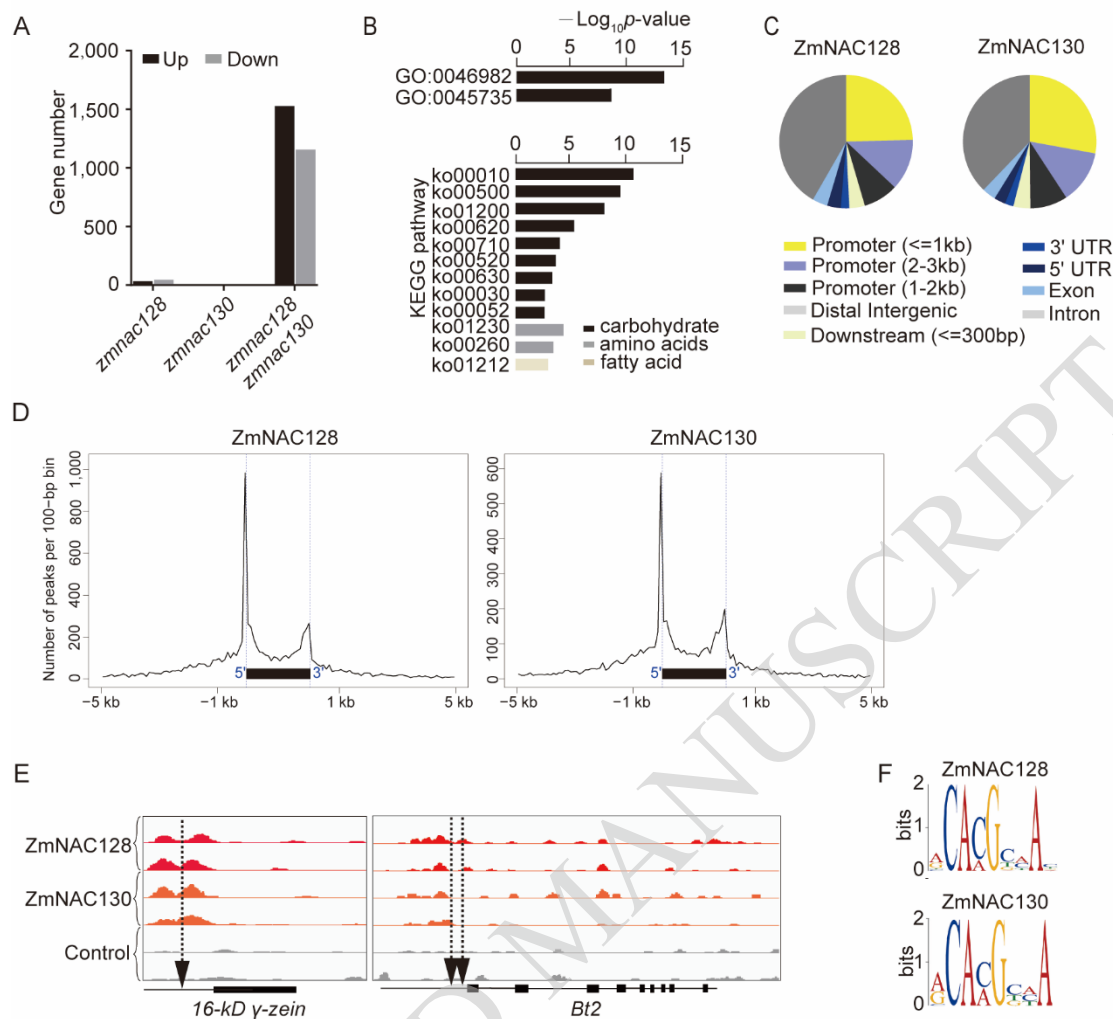


**Figure 2. RNA-seq combined with DAP-seq investigating the direct targets of ZmNAC128 and ZmNAC130.**

**(A)** Number of upregulated and downregulated expressed genes in *zmnac128*, *zmnac130*, and *zmnac128 zmnac130*, compared to the WT. DEGs were identified based on fold-change  $\geq 2$  and  $p$ -value  $\leq 0.05$ .

**(B)** Significantly enriched GO terms and KEGG pathways based on DEGs of *zmnac128 zmnac130*. GO:0046982 (protein heterodimerization activity); GO:0045735 (nutrient reservoir activity); ko00010 (glycolysis/gluconeogenesis); ko00500 (starch and sucrose metabolism); ko01200 (carbon metabolism); ko00620 (pyruvate metabolism); ko00710 (carbon fixation in photosynthetic organisms); ko00520 (amino sugar and nucleotide sugar metabolism); ko00630 (glyoxylate and dicarboxylate metabolism); ko00030 (pentose phosphate pathway); ko00052 (galactose metabolism); ko01230 (biosynthesis of amino acids); ko00260 (glycine, serine and threonine metabolism); ko01212 (fatty acid metabolism).

**(C)** Distribution of ZmNAC128 and ZmNAC130 binding regions in the maize genome. **(D)** Metaplots showing the distribution of ZmNAC128 and ZmNAC130 binding peaks per 100-bp bin corresponding to the  $-1,000$ - to  $+2,000$ -bp region flanking the transcription start site (TSS).

**(E)** IGV shows the distribution of ZmNAC128- and ZmNAC130-binding peaks in the promoters of *16-kD  $\gamma$ -zein* and *Bt2*. For ZmNAC128, ZmNAC130, and IgG (control), two independent

experiments were performed. Aligned reads are indicated in red (ZmNAC128), orange (ZmNAC130), or gray (IgG). The y-axis (or peaks) represents the number (or accumulation) of the aligned reads. The relative positions of the element ACGCAA are marked by arrowheads. **(F)** The most significant elements of ZmNAC128 and ZmNAC130 according to MEME-ChIP analysis.

ACCEPTED MANUSCRIPT

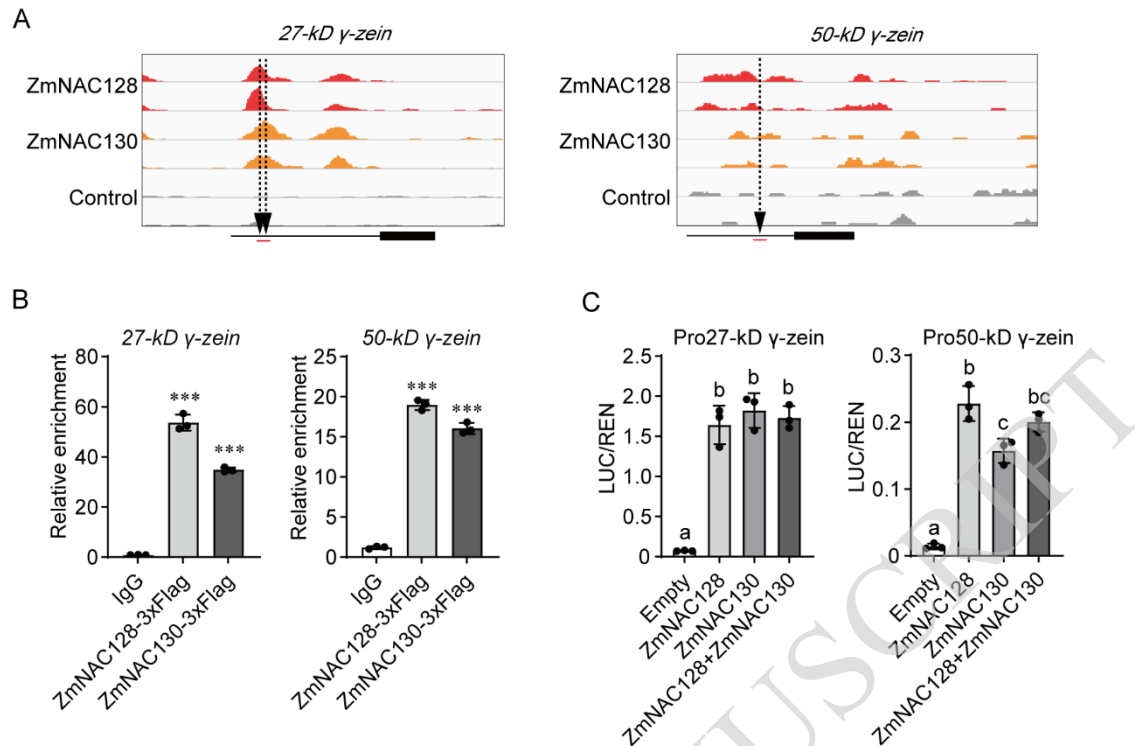


**Figure 3. Verification of 27-kD  $\gamma$ -zein and 50-kD  $\gamma$ -zein as the direct targets of ZmNAC128 and ZmNAC130.**

(A) IGV shows the peaks bound by ZmNAC128 and ZmNAC130 in these two promoters. The relative positions of the element ACGCAA are marked by arrowheads.

(B) ChIP-qPCR detects the *in vivo* binding activities of ZmNAC128 and ZmNAC130 to these two promoters. The red lines under the arrowheads in (A) indicate the region detected by ChIP-qPCR. ChIP products of IgG were used as a negative control. *ACTIN* was used as an internal control.

(C) DLR detects the transactivation activities of ZmNAC128 and ZmNAC130 on the two promoters. The results were also shown in **Supplemental Figure S17**. Data represent means  $\pm$  SD of three independent samples for each test (B and C). Significance differences ( $***p < 0.001$ ) were determined by a Student's *t*-test (B). Different lowercase letters indicate significant differences according to a one-way ANOVA with Tukey's multiple comparisons test ( $p < 0.05$ ) (C).

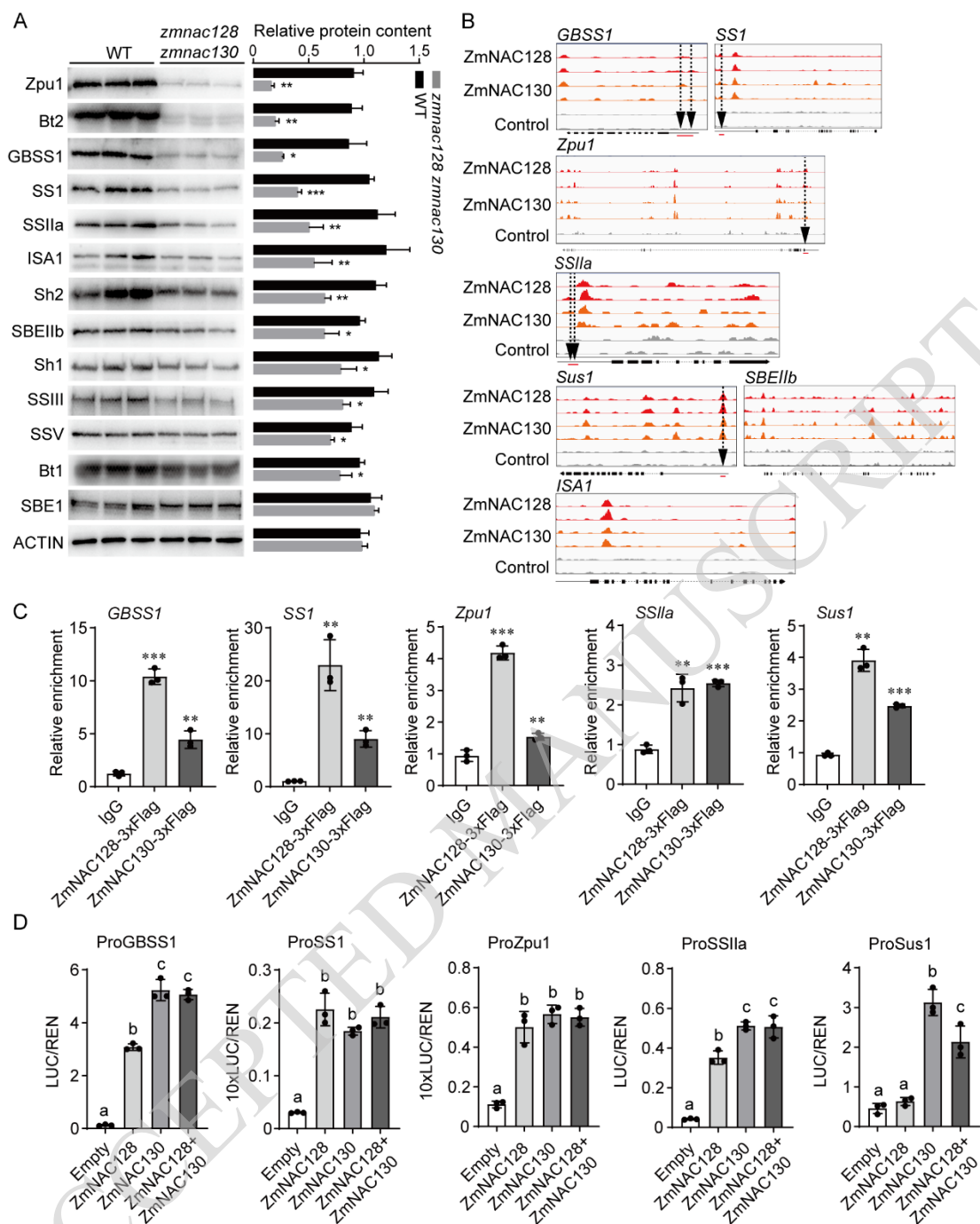


**Figure 4. Verification of starch metabolism genes as direct targets of ZmNAC128 and ZmNAC130.**

(A) Immunoblotting of protein accumulation for the major starch metabolism enzymes in 20-DAP endosperms of *zmnac128 zmnac130* and WT. The 20 ng non-zein proteins per lane were loaded, while ACTIN served as the loading control. The original and intact images were shown in **Supplemental Figure S21**. Three independent samples for each material were performed and quantified by the ImageJ software. For each starch metabolism enzyme, protein abundance in *zmnac128 zmnac130* was normalized to the corresponding WT, which was set to 1.

**(B)** IGV shows binding peaks in the promoters of genes transcriptionally downregulated in *zmnac128 zmnac130*. The relative positions of the cis-element ACGCAA are marked by arrowheads.

**(C)** ChIP-qPCR detects the *in vivo* binding activities of ZmNAC128 and ZmNAC130 to the five promoters. The red lines under the arrowheads in **(B)** indicate the region detected by ChIP-qPCR.

**(D)** DLR detects the transactivation activities of ZmNAC128 and ZmNAC130 on these five promoters. Data represent means  $\pm$  SD of three independent samples for each test (**A**, **C**, and **D**). Significance differences (\*\* $p < 0.01$  and \*\*\* $p < 0.001$ ) were determined by a Student's *t*-test (**A** and **C**). Different lowercase letters indicate significant differences according to a one-way ANOVA with Tukey's multiple comparisons test ( $p < 0.05$ ) (**D**).

ACCEPTED MANUSCRIPT

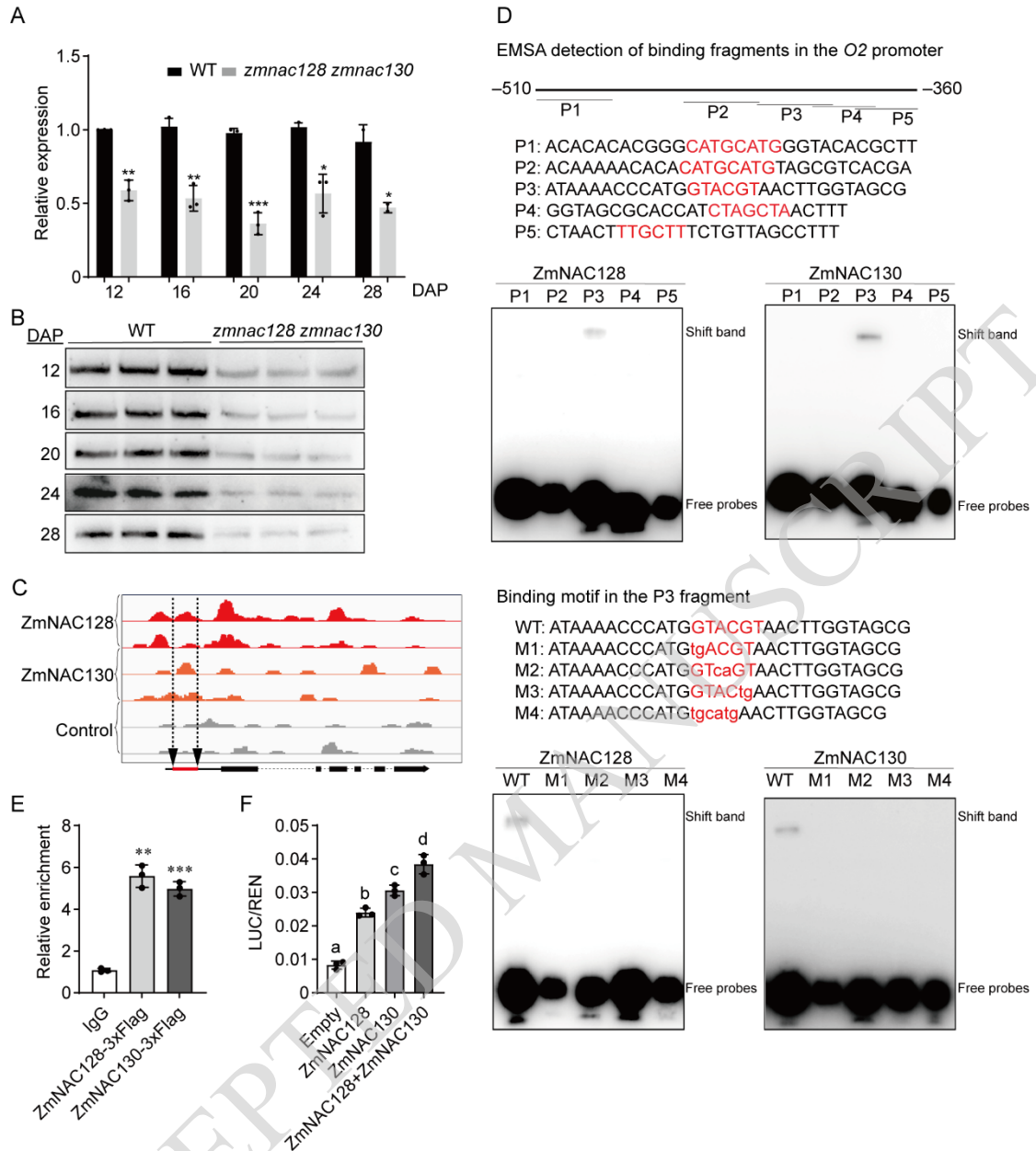


**Figure 5. ZmNAC128 and ZmNAC130 regulate the expression of O2 in the filling endosperm.**

(A) RT-qPCR of O2 expression in the filling endosperms of *zmnac128 zmnac130* and WT. Relative expression was normalized to *ACT1N*. Data represent means  $\pm$  SD of three independent samples for each time point except for two samples at 28 DAP. Statistical significance was determined by a Student's *t*-test. \* $p < 0.05$ , \*\* $p < 0.01$ , \*\*\* $p < 0.001$ .

(B) Immunoblotting of O2 protein in the filling endosperms of *zmnac128 zmnac130* and WT. The 20 ng non-zein proteins per lane were loaded. The quantification was shown in **Supplemental Figure S8**.

(C) IGV shows the peaks bound by ZmNAC128 and ZmNAC130 in the O2 promoter. The relative region covering four candidate elements, CATGCATG, GTACGT, CTAGCTA, and TTGCTT, are marked by a red line in the promoter.



**(D)** EMSA detects an additional cis-element of ZmNAC128 and ZmNAC130 in the O2 promoter. Upside: five biotin-labeled probes in the region of -510 to -360 upstream from the start codon are listed, and candidate cis-elements in the probe sequences are highlighted in red font. Underside: the 6-bp GTACGT box in the P3 probe (WT) and three mutant probes were produced by 2-bp mutations in the 6-bp box.

**(E)** CHIP-qPCR detects the *in vivo* binding activity of ZmNAC128 and ZmNAC130 to the O2 promoter. A red line in the O2 promoter in **(C)** indicates the region detected by CHIP-qPCR.

**(F)** DLR detects the transactivation activities of ZmNAC128 and ZmNAC130 on the O2 promoter. Data represent means  $\pm$  SD of three independent samples for each test (**E** and **F**). Significance differences (\*\* $p < 0.01$  and \*\*\* $p < 0.001$ ) were determined by a Student's *t*-test (**E**). Different lowercase letters indicate significant differences according to a one-way ANOVA with Tukey's multiple comparisons test ( $p < 0.05$ ) (**F**).

ACCEPTED MANUSCRIPT

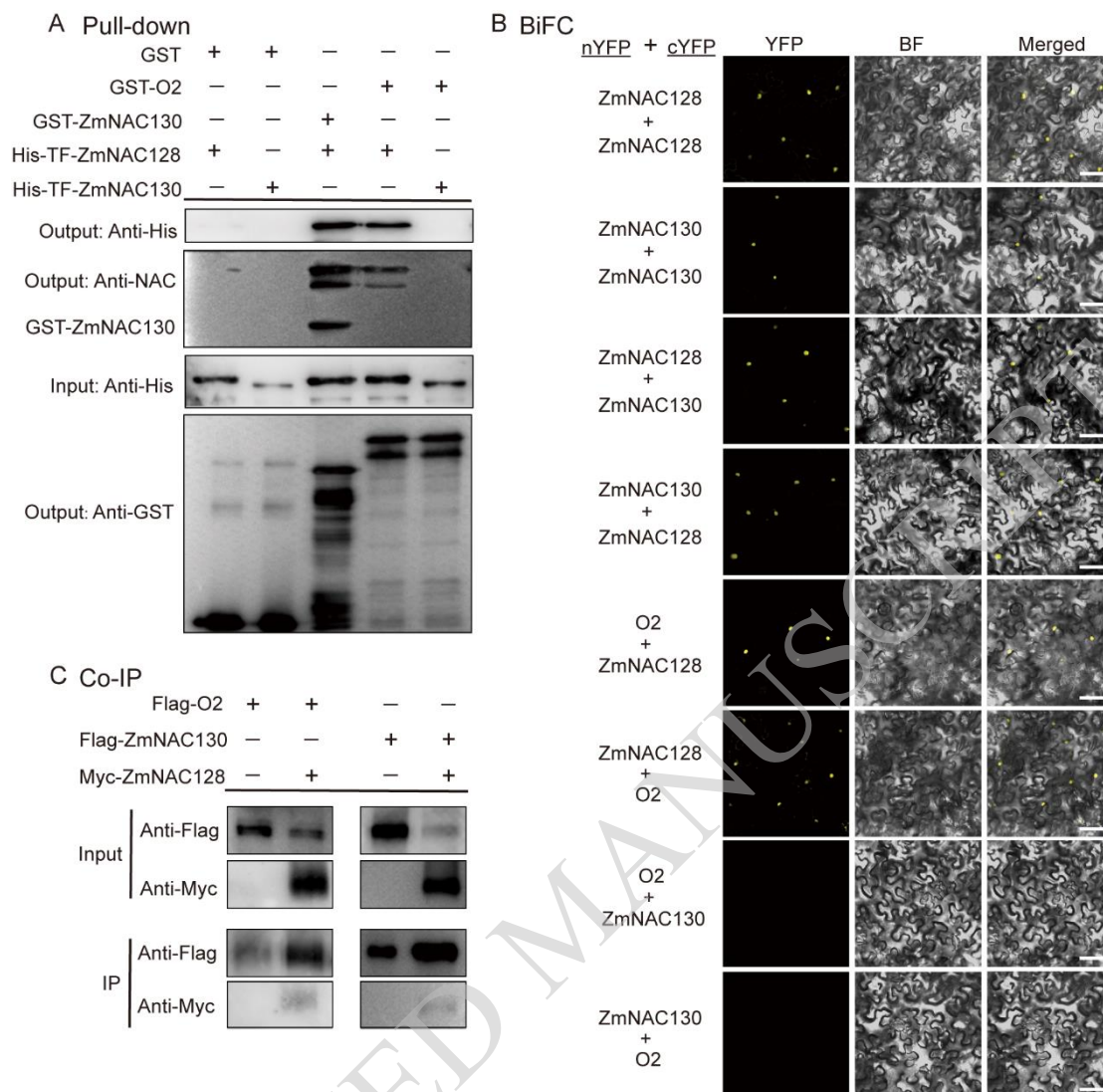


**Figure 6. *In vitro* and *in vivo* protein interaction assays show the physical interaction of O2, ZmNAC128, and ZmNAC130.**

**(A)** GST pull-down detects the interactions between recombinant purified proteins of O2, ZmNAC128, and ZmNAC130.

**(B)** BiFC detects the interactions between O2, ZmNAC128, and ZmNAC130. Negative controls in **Supplemental Figure S11**. BF, bright field. Scale bars, 50  $\mu$ m.

**(C)** Co-IP detects the interactions between O2, ZmNAC128, and ZmNAC130. The indicated plasmids (harboring Flag or Myc tags) were transformed and subsequently co-expressed in *N. benthamiana* leaves. The Flag-fused proteins were immunoprecipitated, and the precipitates were probed with anti-Flag or anti-Myc antibodies.

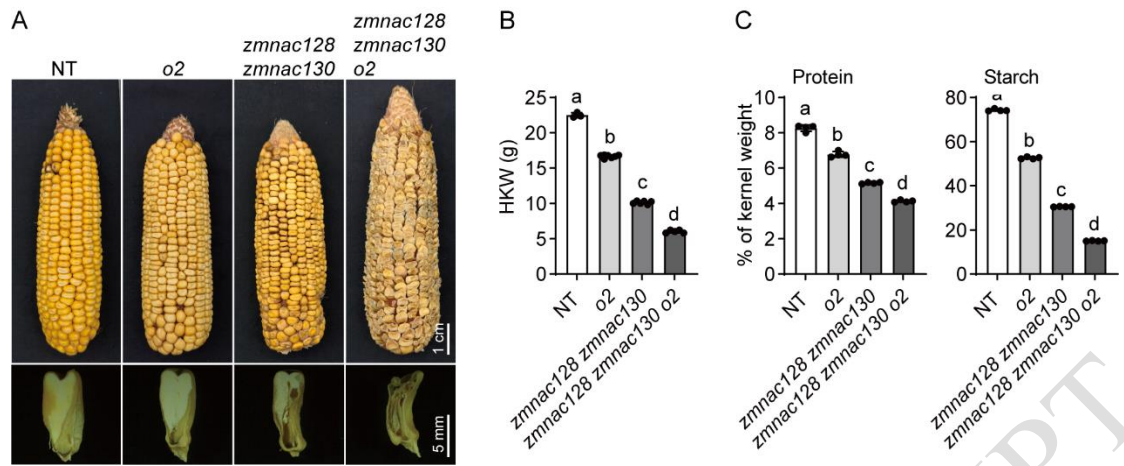


**Figure 7. The triple mutation of *O2*, *ZmNAC128*, and *ZmNAC130* causes a more poorly filled kernel phenotype.**

**(A)** Mature cobs and kernel longitudinal sections of *o2*, *zmnac128 zmnac130*, and *zmnac128 zmnac130 o2* compared to the NT in the KN5585 × B73 background.

**(B)** The hundred-kernel weight (HKW) analysis of the four genetic materials.

**(C)** Determination of protein and starch in the mature kernels from the four genetic materials. Data represent means ± SD of at least three independent samples for each genotype **(B and C)**. Different lowercase letters indicate significant differences according to a one-way ANOVA with Tukey's multiple comparisons test ( $p < 0.05$ ) **(B and C)**.

ACCEPTED MANUSCRIPT

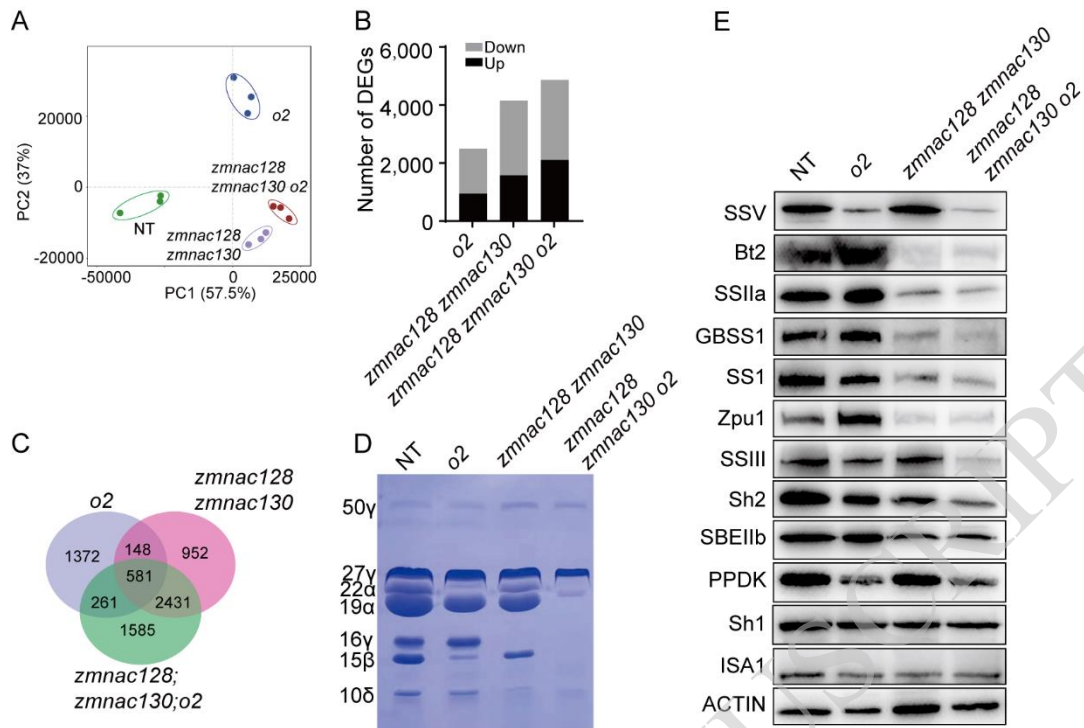


**Figure 8. O2, ZmNAC128, and ZmNAC130 synergistically affect the expression of zeins and starch metabolism enzymes.**

**(A)** Principal component analysis based on transcriptome data of the four genetic materials. There were three independent samples for each genotype.

**(B)** Number of DEGs in *o2*, *zmnac128 zmnac130*, and *zmnac128 zmnac130 o2* compared to the NT. DEGs were identified based on fold-change  $\geq 2$  and  $p$ -value  $\leq 0.05$ .

**(C)** Venn diagram shows the overlap between these DEGs.

**(D)** Coomassie Brilliant Blue staining SDS-PAGE of zein proteins in mature kernels. The total zein proteins loaded in each lane are equal to 200  $\mu$ g of mature kernel flour. Each band was indicated by the corresponding type of zein. 50 $\gamma$ , 50-kD  $\gamma$ -zein; 27 $\gamma$ , 27-kD  $\gamma$ -zein; 22 $\alpha$ , 22-kD  $\alpha$ -zein; 19 $\alpha$ , 19-kD  $\alpha$ -zein; 16 $\gamma$ , 16-kD  $\gamma$ -zein; 15 $\beta$ , 15-kD  $\beta$ -zein; 10 $\delta$ , 10-kD  $\delta$ -zein.

**(E)** Immunoblotting of protein accumulation of starch metabolism enzymes in the 20-DAP endosperm. The 20 ng non-zein proteins for each lane were loaded, while ACTIN was the loading control.

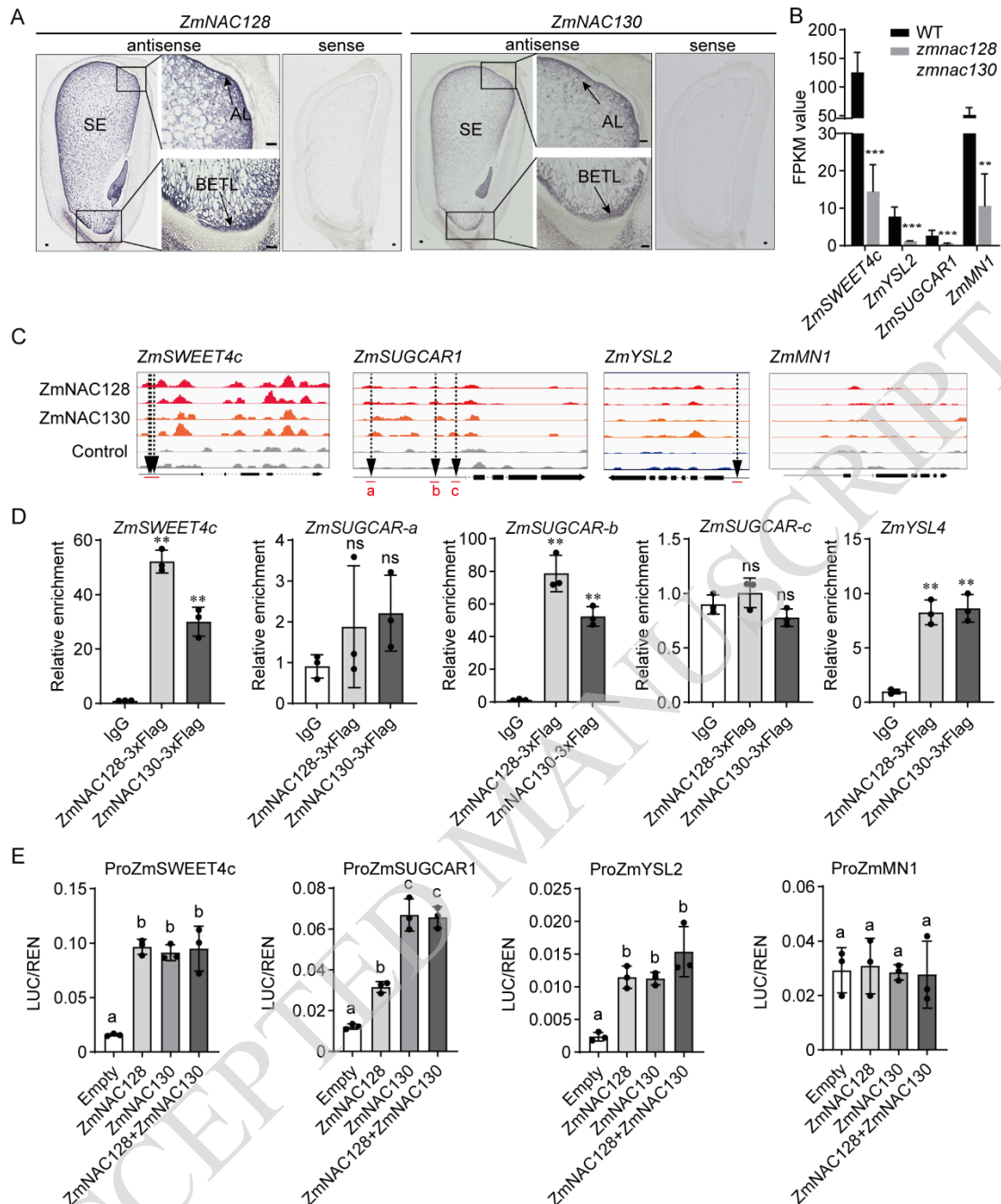


**Figure 9. ZmNAC128 and ZmNAC130 regulate the expression of *ZmSWEET4c*, *ZmSUGCAR1*, and *ZmYSL2*.**

**(A)** RNA *in situ* hybridization of *ZmNAC128* and *ZmNAC130* in 12-DAP B73 kernels. Antisense probes were used to detect the spatial expression of *ZmNAC128* and *ZmNAC130* transcripts. Sense probes were the negative controls. SE, starchy endosperm; AL, aleurone; BETL, basal endosperm transfer layer. Scale bars, 100  $\mu$ m.

**(B)** Expression levels of *ZmSWEET4c*, *ZmSUGCAR1*, *ZmYSL2*, and *ZmMN1* in the 16-DAP endosperms of *zmnac128 zmnac130* versus WT in the KN5585 background. Expression levels are shown as FPKM (fragments per kilobase of exon per million mapped reads). Statistical significance was determined by DESeq2R. \*\* $p < 0.01$ ; \*\*\* $p < 0.001$ .

(C) IGV shows the peaks bound by ZmNAC128 and ZmNAC130 in the four promoters. The relative positions of the element GTACGT are marked by arrowheads.

(D) ChIP-qPCR detects the *in vivo* binding activities of ZmNAC128 and ZmNAC130 to the promoters of *ZmSWEET4c*, *ZmSUGCAR1*, and *ZmYSL2*. The red lines under the arrowheads in (C) indicate the region detected by ChIP-qPCR. Data represent means  $\pm$  SD of three independent samples for each test. Statistical significance was determined by a Student's *t*-test. \*\* $p < 0.01$ ; ns, not significant.

(E) DLR detects the transactivation activities of ZmNAC128, ZmNAC130, and O2 on the four promoters. The data was also shown in **Supplemental Figure S19B** combined with the transactivation of O2, ZmNAC128, and ZmNAC130 on the four promoters. Data represent means  $\pm$  SD of three independent samples for each test. Different lowercase letters indicate significant differences according to a one-way ANOVA with Tukey's multiple comparisons test ( $p < 0.05$ ).

ACCEPTED MANUSCRIPT

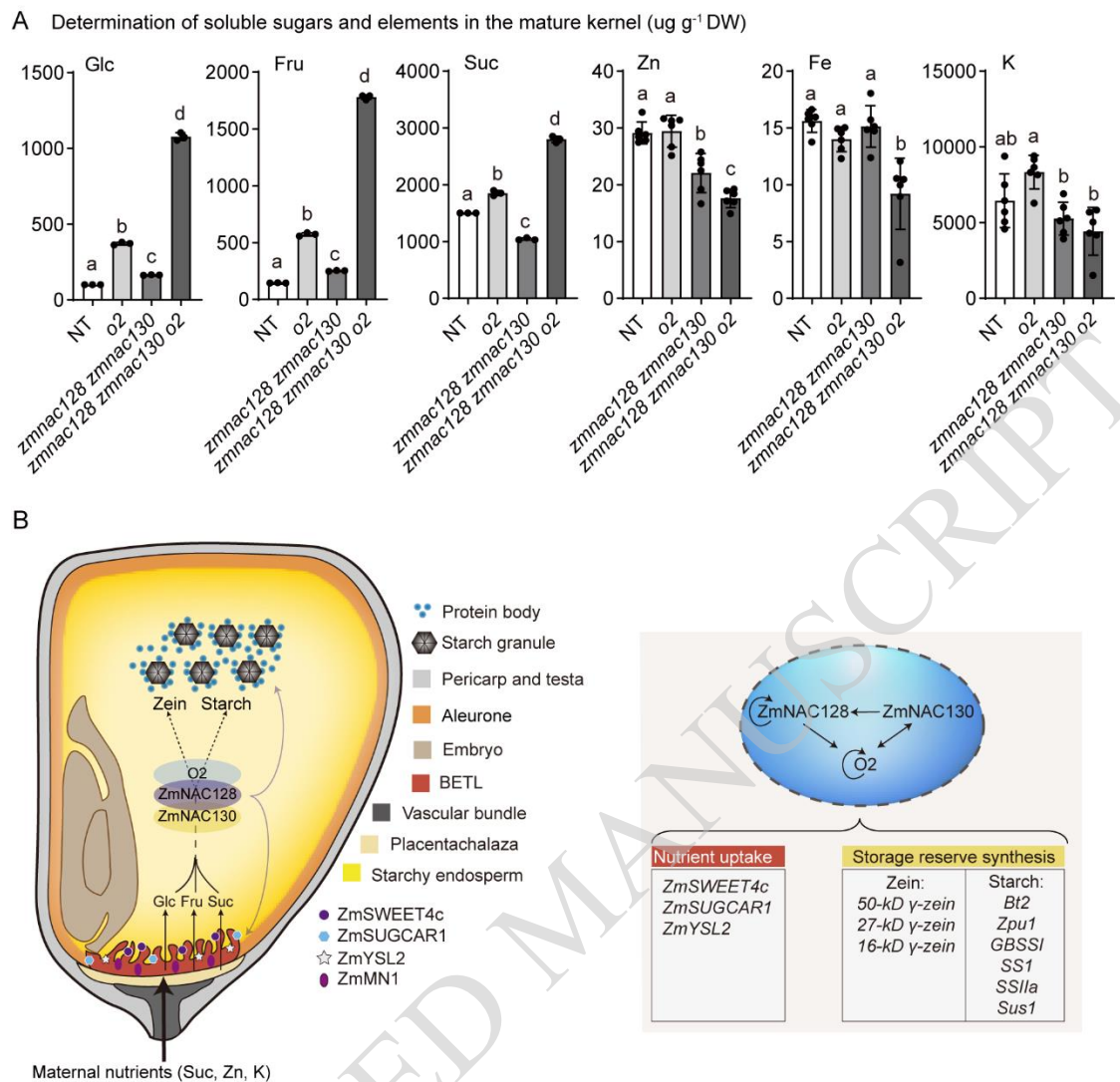


**Figure 10. Mutations in *O2*, *ZmNAC128*, and *ZmNAC130* influence soluble sugar and element levels in kernels, and a working model of these three TFs facilitates endosperm filling.**

**(A)** Determination of soluble sugars (glucose, fructose, and sucrose) and elements (Zn, Fe, and K) in the mature kernels of NT, *o2*, *zmnac128 zmnac130*, and *zmnac128 zmnac130 o2* in the KN5585  $\times$  B73 background. Data represent means  $\pm$  SD of three independent samples in sugar measurement and six independent samples in element measurement for each genotype. Different lowercase letters indicate significant differences according to a one-way ANOVA with Tukey's multiple comparisons test ( $p < 0.05$ ).

**(B)** A working model of *O2*, *ZmNAC128*, and *ZmNAC130* facilitates endosperm filling. Left panel, a cartoon illustration depicts the cooperation of the three TFs to promote endosperm filling. Maternal nutrients are transported via the BETL into the starchy endosperm for synthesis and deposition of storage reserves (starch and zeins). Right panel, the major targets of *ZmNAC128* and *ZmNAC130* have been characterized in this study except for 16-kD  $\gamma$ -zein and *Bt2* which have been previously investigated (Zhang et al., 2019). Arrows indicate direct transcriptional regulation.

## Parsed Citations

- Allen GC, Flores-Vergara MA, Krasynanski S, Kumar S, and Thompson WF (2006). A modified protocol for rapid DNA isolation from plant tissues using cetyltrimethylammonium bromide. *Nat Protoc* 1, 2320-2325.  
Google Scholar: [Author Only](#) [Title Only](#) [Author and Title](#)
- Bartlett A, O'Malley RC, Huang SC, Galli M, Nery JR, Gallavotti A, and Ecker JR (2017). Mapping genome-wide transcription-factor binding sites using DAP-seq. *Nat Protoc* 12, 1659-1672.  
Google Scholar: [Author Only](#) [Title Only](#) [Author and Title](#)
- Becraft PW and Asuncion-Crabb Y (2000). Positional cues specify and maintain aleurone cell fate in maize endosperm development. *Development* 127, 4039-4048.  
Google Scholar: [Author Only](#) [Title Only](#) [Author and Title](#)
- Becraft PW and Gutierrez-Marcos J (2012). Endosperm development: dynamic processes and cellular innovations underlying sibling altruism. *Wiley Interdiscip Rev Dev Biol* 1, 579-593.  
Google Scholar: [Author Only](#) [Title Only](#) [Author and Title](#)
- Becraft PW, Stinard PS, and McCarty DR (1996). CRINKLY4: A TNFR-like receptor kinase involved in maize epidermal differentiation. *Science* 273, 1406-1409.  
Google Scholar: [Author Only](#) [Title Only](#) [Author and Title](#)
- Boston RS and Larkins BA (2009). The Genetics and Biochemistry of Maize Zein Storage Proteins. In *Handbook of Maize: Genetics and Genomics*, J.L. Bennetzen and S. Hake, eds (New York, NY: Springer New York), pp. 715-730.  
Google Scholar: [Author Only](#) [Title Only](#) [Author and Title](#)
- Chao Z, Chen Y, Ji C, Wang Y, Huang X, Zhang C, Yang J, Song T, Wu J, Guo L, Liu C, Han M, Wu Y, Yan J, and Chao D (2022). A genome-wide association study identifies a transporter for zinc uploading to maize kernels. *EMBO Rep*, e55542.  
Google Scholar: [Author Only](#) [Title Only](#) [Author and Title](#)
- Chen J, Zeng B, Zhang M, Xie S, Wang G, Hauck A, and Lai J (2014). Dynamic Transcriptome Landscape of Maize Embryo and Endosperm Development. *Plant Physiol* 166, 252-264.  
Google Scholar: [Author Only](#) [Title Only](#) [Author and Title](#)
- Cheng WH, Taliercio EW, and Chourey PS (1996). The Miniature1 Seed Locus of Maize Encodes a Cell Wall Invertase Required for Normal Development of Endosperm and Maternal Cells in the Pedicel. *Plant Cell* 8, 971-983.  
Google Scholar: [Author Only](#) [Title Only](#) [Author and Title](#)
- Chourey PS and Hueros G (2017). The Basal Endosperm Transfer Layer(BETL): Gateway to the Maize Kernel. In *Maize Kernel Development*, B.A Larkins, ed (Boston, MA: CABI), pp. 56-67.  
Google Scholar: [Author Only](#) [Title Only](#) [Author and Title](#)
- Costa LM, Yuan J, Rouster J, Paul W, Dickinson H, and Gutierrez-Marcos JF (2012). Maternal control of nutrient allocation in plant seeds by genomic imprinting. *Curr Biol* 22, 160-165.  
Google Scholar: [Author Only](#) [Title Only](#) [Author and Title](#)
- Dai D, Ma Z, and Song R (2021). Maize Endosperm Development. *J Integr Plant Biol* 63, 613-627  
Google Scholar: [Author Only](#) [Title Only](#) [Author and Title](#)
- Deng Y, Wang J, Zhang Z, and Wu Y (2020). Transactivation of Sus1 and Sus2 by Opaque2 is an essential supplement to sucrose synthase-mediated endosperm filling in maize. *Plant Biotechnol J* 18, 1897-1907.  
Google Scholar: [Author Only](#) [Title Only](#) [Author and Title](#)
- Feng F, Qi W, Lv Y, Yan S, Xu L, Yang A, Yuan Y, Chen Y, Zhao H, and Song R (2018). OPAQUE11 Is a Central Hub of the Regulatory Network for Maize Endosperm Development and Nutrient Metabolism. *Plant Cell* 30, 375-396.  
Google Scholar: [Author Only](#) [Title Only](#) [Author and Title](#)
- Flint-Garcia SA (2017). Kernel evolution: From teosinte to maize. In *Maize Kernel Development*, B.A Larkins, ed (Boston, MA: CABI), pp. 1-16.  
Google Scholar: [Author Only](#) [Title Only](#) [Author and Title](#)
- Flint-Garcia SA, Bodnar AL, and Scott MP (2009). Wide variability in kernel composition, seed characteristics, and zein profiles among diverse maize inbreds, landraces, and teosinte. *Theoretical and Applied Genetics* 119, 1129-1142.  
Google Scholar: [Author Only](#) [Title Only](#) [Author and Title](#)
- Frame B, Main M, Schick R, and Wang K (2011). Genetic transformation using maize immature zygotic embryos. *Methods Mol Biol* 710, 327-341.  
Google Scholar: [Author Only](#) [Title Only](#) [Author and Title](#)
- Galli M, Khakhar A, Lu Z, Chen Z, Sen S, Joshi T, Nemhauser J, Schmitz R, and Gallavotti A (2018). The DNA binding landscape of



the maize AUXIN RESPONSE FACTOR family. *Nature Communications* 9, 4526.

Google Scholar: [Author Only](#) [Title Only](#) [Author and Title](#)

Gao Y, An K, Guo W, Chen Y, Zhang R, Zhang X, Chang S, Rossi V, Jin F, Cao X, Xin M, Peng H, Hu Z, Guo W, Du J, Ni Z, Sun Q, and Yao Y (2021). The endosperm-specific transcription factor TaNAC019 regulates glutenin and starch accumulation and its elite allele improves wheat grain quality. *Plant Cell* 33, 603-622.

Google Scholar: [Author Only](#) [Title Only](#) [Author and Title](#)

Gomez E, Royo J, Guo Y, Thompson R, and Hueros G (2002). Establishment of cereal endosperm expression domains: identification and properties of a maize transfer cell-specific transcription factor, ZmMRP-1. *Plant Cell* 14, 599-610.

Google Scholar: [Author Only](#) [Title Only](#) [Author and Title](#)

Gomez E, Royo J, Muniz LM, Sellam O, Paul W, Gerentes D, Barrero C, Lopez M, Perez P, and Hueros G (2009). The Maize Transcription Factor Myb-Related Protein-1 Is a Key Regulator of the Differentiation of Transfer Cells. *Plant Cell* 21, 2022-2035.

Google Scholar: [Author Only](#) [Title Only](#) [Author and Title](#)

Gontarek BC, Neelakandan AK, Wu H, and Becraft PW (2016). NKD Transcription Factors Are Central Regulators of Maize Endosperm Development. *Plant Cell* 28, 2916-2936.

Google Scholar: [Author Only](#) [Title Only](#) [Author and Title](#)

Guan H, Dong Y, Lu S, Liu T, He C, Liu C, Liu Q, Dong R, Wang J, Li Y, Qi S, and Wang L (2020). Characterization and map-based cloning of miniature2-m1, a gene controlling kernel size in maize. *J Integr Agric* 19, 1961-1973.

Google Scholar: [Author Only](#) [Title Only](#) [Author and Title](#)

Hannah LC and Boehlein S (2017). Starch biosynthesis in maize endosperm. In *Maize kernel development*, B.A Larkins, ed (Boston, MA: CABI), pp. 149-159.

Google Scholar: [Author Only](#) [Title Only](#) [Author and Title](#)

He Y, Yang Q, Yang J, Wang Y, Sun X, Wang S, Qi W, Ma Z, and Song R (2021). shrunken4 is a mutant allele of ZmYSL2 that affects aleurone development and starch synthesis in maize. *Genetics* 218, iyab070.

Google Scholar: [Author Only](#) [Title Only](#) [Author and Title](#)

Huang J, Xu W, Zhai J, Hu Y, Guo J, Zhang C, Zhao Y, Zhang L, Martine C, Ma H, Huang C (2023). Nuclear phylogeny and insights into whole-genome duplications and reproductive development of Solanaceae plants. *Plant Communications*, 100595

Google Scholar: [Author Only](#) [Title Only](#) [Author and Title](#)

Huang L, Tan H, Zhang C, Li Q, and Liu Q (2021). Starch biosynthesis in cereal endosperms: An updated review over the last decade. *Plant Commun* 2, 100237.

Google Scholar: [Author Only](#) [Title Only](#) [Author and Title](#)

Jin P, Guo T, and Becraft PW (2000). The maize CR4 receptor-like kinase mediates a growth factor-like differentiation response. *Genesis* 27, 104-116. Kim D, Langmead B, Salzberg SL (2015) HISAT: a fast spliced aligner with low memory requirements. *Nature Methods* 12, 357-360.

Google Scholar: [Author Only](#) [Title Only](#) [Author and Title](#)

Larkins BA, Wu Y, Song R, and Messing J (2017). Maize seed storage proteins. In *Maize kernel development*, B.A Larkins, ed (Boston, MA: CABI), pp. 157-189.

Google Scholar: [Author Only](#) [Title Only](#) [Author and Title](#)

Lending CR and Larkins BA (1989). Changes in the zein composition of protein bodies during maize endosperm development. *Plant Cell* 1, 1011-1023.

Google Scholar: [Author Only](#) [Title Only](#) [Author and Title](#)

Leroux BM, Goodyke AJ, Schumacher KI, Abbott CP, Clore AM, Yadegari R, Larkins BA, and Dannenhoffer JM (2014). Maize early endosperm growth and development: from fertilization through cell type differentiation. *Am J Bot* 101, 1259-1274.

Google Scholar: [Author Only](#) [Title Only](#) [Author and Title](#)

Li C and Song R (2020). The regulation of zein biosynthesis in maize endosperm. *Theor Appl Genet* 133, 1443-1453.

Google Scholar: [Author Only](#) [Title Only](#) [Author and Title](#)

Li C, Yue Y, Chen H, Qi W, and Song R (2018). The ZmbZIP22 Transcription Factor Regulates 27-kD gamma-Zein Gene Transcription during Maize Endosperm Development. *The Plant Cell* 30, 2402-2424.

Google Scholar: [Author Only](#) [Title Only](#) [Author and Title](#)

Li C, Qiao Z, Qi W, Wang Q, Yuan Y, Yang X, Tang Y, Mei B, Lv Y, Zhao H, Xiao H, and Song R (2015). Genome-Wide Characterization of cis-Acting DNA Targets Reveals the Transcriptional Regulatory Framework of Opaque2 in Maize. *The Plant Cell* 27, 532-545.

Google Scholar: [Author Only](#) [Title Only](#) [Author and Title](#)

Li Q and Wu Y (2020). The encyclopedia of maize kernel gene expression. *J Integr Plant Biol* 62, 879-881.

Google Scholar: [Author Only](#) [Title Only](#) [Author and Title](#)

Lid SE, Gruis D, Jung R, Lorentzen JA, Ananiev E, Chamberlin M, Niu X, Meeley R, Nichols S, and Olsen OA (2002). The defective kernel 1 (*dek1*) gene required for aleurone cell development in the endosperm of maize grains encodes a membrane protein of the calpain gene superfamily. *Proc Natl Acad Sci U S A* 99, 5460-5465.

Google Scholar: [Author Only](#) [Title Only](#) [Author and Title](#)

Liu Y, Hou J, Wang X, Li T, Majeed U, Hao C, and Zhang X (2020). The NAC transcription factor NAC019-A1 is a negative regulator of starch synthesis in wheat developing endosperm. *J Exp Bot* 71, 5794-5807.

Google Scholar: [Author Only](#) [Title Only](#) [Author and Title](#)

Livak KJ and Schmittgen TD (2001). Analysis of Relative Gene Expression Data Using Real-Time Quantitative PCR and the 2- $\Delta\Delta$ CT Method. *Methods* 25, 402-408.

Google Scholar: [Author Only](#) [Title Only](#) [Author and Title](#)

Lynch JM and Barbano DM (1999). Kjeldahl Nitrogen Analysis as a Reference Method for Protein Determination in Dairy Products. *Journal of AOAC INTERNATIONAL* 82, 1389-1398.

Google Scholar: [Author Only](#) [Title Only](#) [Author and Title](#)

Lohmer S, Maddaloni M, Motto M, Di Fonzo N, Hartings H, Salamini F, and Thompson RD (1991). The maize regulatory locus Opaque-2 encodes a DNA-binding protein which activates the transcription of the b-32 gene. *Embo J* 10, 617-624.

Google Scholar: [Author Only](#) [Title Only](#) [Author and Title](#)

Love MI, Huber W, and Anders S (2014). Moderated estimation of fold change and dispersion for RNA-seq data with DESeq2. *Genome Biol* 15, 550.

Google Scholar: [Author Only](#) [Title Only](#) [Author and Title](#)

Ning L, Wang Y, Shi X, Zhou L, Ge M, Liang S, Wu Y, Zhang T, and Zhao H (2022). Nitrogen-dependent binding of the transcription factor PBF1 contributes to the balance of protein and carbohydrate storage in maize endosperm. *Plant Cell* 35, 409-434

Google Scholar: [Author Only](#) [Title Only](#) [Author and Title](#)

O'Malley RC, Huang SC, Song L, Lewsey MG, Bartlett A, Nery JR, Galli M, Gallavotti A, and Ecker JR (2016). Cistrome and Epicistrome Features Shape the Regulatory DNA Landscape. *Cell* 166, 1598.

Google Scholar: [Author Only](#) [Title Only](#) [Author and Title](#)

Olsen OA (2001). ENDOSPERM DEVELOPMENT: Cellularization and Cell Fate Specification. *Annu Rev Plant Physiol Plant Mol Biol* 52, 233-267.

Google Scholar: [Author Only](#) [Title Only](#) [Author and Title](#)

Pysh LD, Aukerman MJ, and Schmidt RJ (1993). OHP1: a maize basic domain/leucine zipper protein that interacts with opaque2. *The Plant Cell* 5, 227-236.

Google Scholar: [Author Only](#) [Title Only](#) [Author and Title](#)

Qiao Z, Qi W, Wang Q, Feng Y, Yang Q, Zhang N, Wang S, Tang Y, and Song R (2016). ZmMADS47 Regulates Zein Gene Transcription through Interaction with Opaque2. *Plos Genetics* 12, 1005991.

Google Scholar: [Author Only](#) [Title Only](#) [Author and Title](#)

Sabelli PA and Larkins BA (2009). The development of endosperm in grasses. *Plant Physiol* 149, 14-26.

Google Scholar: [Author Only](#) [Title Only](#) [Author and Title](#)

Schmidt RJ, Burr FA, and Burr B (1987). Transposon tagging and molecular analysis of the maize regulatory locus opaque-2. *Science* 238, 960-963.

Google Scholar: [Author Only](#) [Title Only](#) [Author and Title](#)

Schmidt RJ, Burr FA, Aukerman MJ, and Burr B (1990). Maize Regulatory Gene Opaque-2 Encodes a Protein with a Leucine-Zipper Motif That Binds to Zein DNA. *Proc Natl Acad Sci USA* 87, 46-50.

Google Scholar: [Author Only](#) [Title Only](#) [Author and Title](#)

Shen B, Li C, Min Z, Meeley RB, Tarczynski MC, and Olsen OA (2003). *sal1* determines the number of aleurone cell layers in maize endosperm and encodes a class E vacuolar sorting protein. *Proc Natl Acad Sci U S A* 100, 6552-6557.

Google Scholar: [Author Only](#) [Title Only](#) [Author and Title](#)

Sosso D, Luo D, Li Q, Sasse J, Yang J, Gendrot G, Suzuki M, Koch KE, McCarty DR, Chourey PS, Rogowsky PM, Ross-Ibarra J, Yang B, and Frommer WB (2015). Seed filling in domesticated maize and rice depends on SWEET-mediated hexose transport. *Nat Genet* 47, 1489-1493.

Google Scholar: [Author Only](#) [Title Only](#) [Author and Title](#)

VicenteCarbajosa J, Moose SP, Parsons RL, and Schmidt RJ (1997). A maize zinc-finger protein binds the prolamin box in zein gene promoters and interacts with the basic leucine zipper transcriptional activator Opaque2. *Proc Natl Acad Sci USA* 94, 7685-7690.

Google Scholar: [Author Only](#) [Title Only](#) [Author and Title](#)

Wang E, Wang J, Zhu X, Hao W, Wang L, Li Q, Zhang L, He W, Lu B, Lin H, Ma H, Zhang G, and He Z (2008). Control of rice grain-filling and yield by a gene with a potential signature of domestication. *Nat Genet* 40, 1370-1374.

Google Scholar: [Author Only](#) [Title Only](#) [Author and Title](#)

Wang J, Chen Z, Zhang Q, Meng S, and Wei C (2020). The NAC Transcription Factors OsNAC20 and OsNAC26 Regulate Starch and Storage Protein Synthesis. *Plant Physiol* 184, 1775-1791.

Google Scholar: [Author Only](#) [Title Only](#) [Author and Title](#)

Wei Y, Ren Z, Wang B, Zhang L, Zhao Y, Wu J, Li L, Zhang X, and Zhao X (2021). A nitrate transporter encoded by ZmNPF7.9 is essential for maize seed development. *Plant Sci* 308, 110901.

Google Scholar: [Author Only](#) [Title Only](#) [Author and Title](#)

Widiez T, Ingram GC, and F., G.-M.J. (2017). Embryo–Endosperm–Sporophyte Interactions in Maize Seeds. In *Maize Kernel Development*, B.A Larkins, ed (Boston, MA: CABI), pp. 108-118.

Google Scholar: [Author Only](#) [Title Only](#) [Author and Title](#)

Wu Y and Messing J (2012). Rapid Divergence of Prolamin Gene Promoters of Maize After Gene Amplification and Dispersal. *Genetics* 192, 507-519.

Google Scholar: [Author Only](#) [Title Only](#) [Author and Title](#)

Wu Y, Holding DR, and Messing J (2010). gamma-Zeins are essential for endosperm modification in quality protein maize. *Proc Natl Acad Sci USA* 107, 12810-12815.

Google Scholar: [Author Only](#) [Title Only](#) [Author and Title](#)

Xin M, Yang R, Li G, Chen H, Laurie J, Ma C, Wang D, Yao Y, Larkins BA, Sun Q, Yadegari R, Wang X, and Ni Z (2013). Dynamic expression of imprinted genes associates with maternally controlled nutrient allocation during maize endosperm development. *Plant Cell* 25, 3212-3227.

Google Scholar: [Author Only](#) [Title Only](#) [Author and Title](#)

Xu J and Messing J (2008). Organization of the prolamin gene family provides insight into the evolution of the maize genome and gene duplications in grass species. *Proc Natl Acad Sci USA* 105, 14330-14335.

Google Scholar: [Author Only](#) [Title Only](#) [Author and Title](#)

Yang B, Wang J, Yu M, Zhang M, Zhong Y, Wang T, Liu P, Song W, Zhao H, Fastner A, Suter M, Rentsch D, Ludewig U, Jin W, Geiger D, Hedrich R, Braun DM, Koch KE, McCarty DR, Wu W, Li X, Wang Y, and Lai J (2022). The sugar transporter ZmSUGCAR1 of the Nitrate Transporter 1/Peptide Transporter family is critical for maize grain filling. *Plant Cell* 34, 4232-4254.

Google Scholar: [Author Only](#) [Title Only](#) [Author and Title](#)

Yang T, Wu X, Wang W, and Wu Y (2023). Regulation of seed storage protein synthesis in monocot and dicot plants: A comparative review. *Mol Plant* 16, 145-167.

Google Scholar: [Author Only](#) [Title Only](#) [Author and Title](#)

Yang T, Guo L, Ji C, Wang H, Wang J, Zheng X, Xiao Q, and Wu Y (2021). The B3 domain-containing transcription factor ZmABI19 coordinates expression of key factors required for maize seed development and grain filling. *Plant Cell* 33, 104-128.

Google Scholar: [Author Only](#) [Title Only](#) [Author and Title](#)

Yang T, Wang H, Guo L, Wu X, Xiao Q, Wang J, Wang Q, Ma G, Wang W, and Wu Y (2022). ABA-induced Phosphorylation of basic Leucine Zipper 29, ABSCISIC ACID INSENSITIVE 19 and Opaque2 by SnRK2.2 Enhances Gene Transactivation for Endosperm Filling in Maize. *Plant Cell* 34, 1933-1956.

Google Scholar: [Author Only](#) [Title Only](#) [Author and Title](#)

Yi F, Gu W, Chen J, Song N, Gao X, Zhang X, Zhou Y, Ma X, Song W, Zhao H, Esteban E, Pasha A, Provart NJ, and Lai J (2019). High Temporal-Resolution Transcriptome Landscape of Early Maize Seed Development. *Plant Cell* 31, 974-992.

Google Scholar: [Author Only](#) [Title Only](#) [Author and Title](#)

Yi G, Lauter AM, Scott MP, and Becraft PW (2011). The thick aleurone1 mutant defines a negative regulation of maize aleurone cell fate that functions downstream of defective kernel1. *Plant Physiol* 156, 1826-1836.

Google Scholar: [Author Only](#) [Title Only](#) [Author and Title](#)

Yi G, Neelakandan AK, Gontarek BC, Vollbrecht E, and Becraft PW (2015). The naked endosperm genes encode duplicate INDETERMINATE domain transcription factors required for maize endosperm cell patterning and differentiation. *Plant Physiol* 167, 443-456.

Google Scholar: [Author Only](#) [Title Only](#) [Author and Title](#)

Zhan J, Dannenhoffer JM, and Yadegari R (2017). Endosperm Development and Cell Specialization. In *Maize Kernel Development*, B.A Larkins, ed (Boston, MA: CABI), pp. 28-43.

Google Scholar: [Author Only](#) [Title Only](#) [Author and Title](#)

Zhan J, Li G, Ryu CH, Ma C, Zhang S, Lloyd A, Hunter BG, Larkins BA, Drews GN, Wang X, and Yadegari R (2018). Opaque-2 Regulates a Complex Gene Network Associated with Cell Differentiation and Storage Functions of Maize Endosperm. *The Plant*

Cell 30, 2425-2446.

Google Scholar: [Author Only](#) [Title Only](#) [Author and Title](#)

Zhan J, Thakare D, Ma C, Lloyd A, Nixon NM, Arakaki AM, Burnett WJ, Logan KO, Wang D, Wang X, Drews G, and Yadegaria R (2015). RNA Sequencing of Laser-Capture Microdissected Compartments of the Maize Kernel Identifies Regulatory Modules Associated with Endosperm Cell Differentiation. *Plant Cell* 27, 513-531.

Google Scholar: [Author Only](#) [Title Only](#) [Author and Title](#)

Zhang Y, Liu T, Meyer CA, Eeckhoute J, Johnson DS, Bernstein BE, Nusbaum C, Myers RM, Brown M, Li W, Liu XS (2008). Model-based analysis of ChIP-Seq (MACS). *Genome Biology* 9, R137. Zhang Z, Yang J, and Wu Y (2015). Transcriptional Regulation of Zein Gene Expression in Maize through the Additive and Synergistic Action of opaque2, Prolamine-Box Binding Factor, and O2 Heterodimerizing Proteins. *The Plant Cell* 27, 1162-1172.

Google Scholar: [Author Only](#) [Title Only](#) [Author and Title](#)

Zhang Z, Zheng X, Yang J, Messing J, and Wu Y (2016). Maize endosperm-specific transcription factors O2 and PBF network the regulation of protein and starch synthesis. *Proc Natl Acad Sci U S A* 113, 10842-10847.

Google Scholar: [Author Only](#) [Title Only](#) [Author and Title](#)

Zhang Z, Dong J, Ji C, Wu Y, and Messing J (2019). NAC-type transcription factors regulate accumulation of starch and protein in maize seeds. *Proc Natl Acad Sci USA* 116, 11223-11228.

Google Scholar: [Author Only](#) [Title Only](#) [Author and Title](#)

Zhou L, Liu C, Chen Q, Wang W, Yao S, Zhao Z, Zhu S, Hong X, Xiong Y, and Cai Y (2021). Fine mapping and candidate gene analysis of maize defective kernel mutant dek54. *Acta Agron Sin* 47, 1903–1912.

Google Scholar: [Author Only](#) [Title Only](#) [Author and Title](#)

ACCEPTED MANUSCRIPT